Research

Advanced Materials and Materials Genome—Review

Recent Developments in Functional Crystals in China

Jiyang Wang[1*], Haohai Yu[1], Yicheng Wu[2], Robert Boughton[3]

ABSTRACT Functional crystals are the basic materials for the development of modern science and technology and are playing key roles in the modern information era. In this paper, we review functional crystals in China, including research history, significant achievements, and important applications by highlighting the most recent progress in research. Challenges for the development of functional materials are discussed and possible directions for development are proposed by focusing on potential strengths of these materials.

1 Introduction

Crystals are solid materials with long-range order. Those that exhibit functional properties, such as laser activity, nonlinear optical (NLO) properties, piezoelectric properties, and so forth, are called "functional crystals." Diamond is not only a well-known precious stone, but also a good functional crystal due to its extreme hardness and superior heat and electrical conduction. Silicon is the most widely used semiconductor crystal for creating the integrated circuits that have allowed computers to function as the foundation of our modern world. In 1900, corundum crystals were artificially grown in France, and were used to manufacture watch bearings, opening a new era for the application of functional crystals. Different from natural crystals, artificial crystals are high-tech materials with high purity and high perfection that are engineered for desired applications. Such applications mainly include functional properties that transform one form of energy, such as sonic, light, heat, electrical, magnetic, and so forth, into another. In modern science and technology, artificial crystals play key roles, and are called functional synthetic crystals. In this paper, we will give a brief review of some functional synthetic crystals, focusing on laser and nonlinear crystals that are related to the manufacture of solid-state la-

sers.

In 1960, Maiman invented the first laser using a ruby crystal (Cr^{3+}:Al_2O_3) as the laser medium; this device opened vast new horizons for quantum electronics [1]. The laser crystal is the core and foundation of the development of laser technology. In the 1970s, a neodymium-doped yttrium aluminum garnet (Nd:YAG) laser crystal was developed and widely adopted due to its superior laser characteristics and high thermal conductivity. In the 1980s, a titanium-doped sapphire (Ti:Al_2O_3) was grown, and a tunable laser (with a range of 660–1100 nm) was developed. This tunable laser formed the foundation for ultra-fast, ultra-short-pulse high-intensity lasers, resulting in the development of femtosecond (fs)-pulsed lasers. The commercialization of the laser diode during the late 1980s caused the rapid development of all-solid-state lasers, which in turn promoted a great increase in laser applications and in laser technology itself. In the 1990s, the successful growth of a neodymium-doped yttrium orthovanadate (Nd:YVO$_4$) crystal made miniature pocket lasers possible.

A particular laser can emit only at a specific wavelength, which can in turn be converted to another wavelength by using NLO crystals. When laser radiation passes through the nonlinear medium, the nonlinear response to light-induced polarization of the electromagnetic field feeds back to the input light wave, resulting in the generation of harmonics at a particular wavelength by means of a nonlinear effect. This effect, which is related to the laser intensity, differs from linear optical effects and is referred to as a NLO effect. Crystals possessing NLO effects are called NLO crystals.

Functional crystals can be divided into several categories, such as laser media, NLO crystals, electro-optical (EO) crystals, piezoelectric crystals, pyroelectric crystals, and so forth, according to the principal effect of the crystal and its application. In addition, most of the substrates used as semiconductors are functional crystals. Although the crystal volume in most electronics equipment is small, their functional effect is quite important.

In this review, recent progress in the development of func-

1 State Key Laboratory of Crystal Materials, Shandong University, Jinan 250100, China; 2 Technical Institute of Physics and Chemistry, Chinese Academy of Sciences, Beijing 100080, China; 3 Department of Physics and Astronomy, Bowling Green State University, Bowling Green, OH 43403-0001, USA
* Correspondence author. E-mail: jywang@sdu.edu.cn

tional crystals in China is summarized.

Special attention has been paid to large, high-quality garnets, including neodymium and other rare earth ion-doped crystals that still maintain top priority in the development of laser media applications. The research and testing of transparent laser ceramics and micro-crystalline glasses are also going forward. A series of micro-chip laser crystals have been developed to meet the requirements of miniature lasers. Different kinds of NLO crystals that are suitable for use in the ultraviolet/visible/near-infrared (IR) spectral regions have been developed, and new NLO crystals that can be used in the far-IR to THz wave regions are topics of recent development in this field. To meet ever-growing needs in the mid-IR (e.g., near 2 μm) range, directly pumped laser crystals, Raman shift crystals, and mid-IR NLO crystals all fulfill the requirements. Along with the development of large potassium dihydrogen phosphate (KDP) and deuterated potassium dihydrogen phosphate (DKDP) crystals, large lithium triborate (LBO) and yttrium calcium oxyborate (YCOB) crystals have attracted a great deal of attention. Consequently, more research activity must also be devoted to improving crystal-growth technology in order to mass-produce high-quality crystals at low cost.

Scintillation crystals are very important in high-energy physics and medical diagnosis. Developments in this field are focused on the design and growth of new crystals that possess excellent scintillation response and that can expand the application of these crystals.

Recently, the extension of microstructure physics has become more pervasive, with a stronger influence on crystal technology than ever before. The microstructure of photoelectronic functional materials represents the intersection of materials science, condensed matter physics, and photoelectronic technology, and has profound scientific and technological significance. A great deal of progress in research on dielectric superlattices has been made in both fundamental and technological terms in recent years.

The progress made in this field will be reviewed in the following sections.

2 Present status of and progress in functional crystals

2.1 Laser crystals

A laser crystal is the fundamental material for constructing an all-solid-state laser. Laser crystals are crystals that can be electrically or optically pumped in order to produce efficient laser output. A laser crystal is normally composed of a matrix and an emitting light center, which can take the form of a rare earth ion, a transition metal ion, or some other sources such as a color center .

The earliest known laser output was obtained with chromium-doped ruby ($Cr:Al_2O_3$) in 1960. Since then, a variety of laser crystals with more than 350 different matrix materials and with more than 20 different kinds of emitting ions have been developed, and efficient laser output has been obtained at more than 70 different wavelengths. Laser crystals can be divided into three main groups: oxide crystals (e.g., Al_2O_3,

$Y_3Al_5O_{12}$, $YAlO_3$, Y_2O_3, Sc_2O_3), fluoride crystals (e.g., CaF_2, BaF_2, SrF_2, LaF_3, MgF_2, $LiYF_4$, LiCAF, LiSAF), and metal oxysalt crystals (e.g., $Ca_5(PO_4)_3F$, Y_2SiO_5, YVO_4, $YAl_3(BO_3)_4$, $CaWO_4$). Among these, the most widely used crystals are the three basic laser crystals: Nd:YAG, $Nd:YVO_4$, and $Ti:Al_2O_3$. The Nd:YAG crystal is used to manufacture high- and medium-power output lasers; the $Nd:YVO_4$ crystal is used for miniature low-power output lasers; and the $Ti:Al_2O_3$ crystal is used for tunable ultra-fast output lasers. Apart from these three, some new laser crystals have been developed in recent years that hold promise for potential applications in meeting the growing requirements for all-solid-state lasers and the needs of the related high-tech industry.

2.1.1 Garnet laser crystals

Garnet is a natural mineral that has been studied for many years. Based on its internal structure, the garnet crystal belongs to the cubic system, with the general formula $A_3B_2C_3O_{12}$, where A is an atom such as Y, Gd, Lu, or La that occupies a site in the dodecahedron; B is an atom such as Sc, Al, Ga, or Fe that occupies a site in the octahedron; and C is an atom such as Al, Ga, or Fe that is located on a tetrahedral site. The important garnet crystals include YAG, yttrium gallium garnet (YGG), and gadolinium gallium garnet (GGG). YAG is one of the most widely used laser host crystals.

The Y—O bond in the YAG crystal is 0.245 nm in length. Since Y^{3+} and other rare earth ions have similar radii, the Y^{3+} ions at the dodecahedron sites can be replaced by other trivalent rare earth cations, including Nd^{3+}, Er^{3+}, Tm^{3+}, Ho^{3+}, and Yb^{3+}, as the active ions for lasing. In addition, ions at sites in the octahedron can be replaced by trivalent metal ions such as Cr^{3+}, V^{3+}, Mn^{3+}, and Fe^{3+} acting as sensitizers. Currently, Nd^{3+}:YAG, (Nd^{3+}, Ce^{3+}):YAG, (Nd^{3+}, Ce^{3+}):Tb^{3+}:YAG, and (Nd^{3+}, Ce^{3+}):Cr^{3+}:YAG are the most common laser materials in this class. To be classified as an excellent laser material, the host crystal should possess good mechanical, thermal, and optical properties. Table 1 lists the physical, chemical, and thermal properties of YAG [2], which is considered to be a model for laser crystals. The main disadvantage of Nd:YAG is the low doping concentration and the narrow absorption-spectrum peaks, both of which indicate that any further improvement in laser efficiency when pumped with a laser diode is difficult.

Since Geusic et al. first reported the laser output of the Nd:YAG crystal in 1964 [3], Nd:YAG crystals and the lasers built with them have attracted a great deal of research interest. Today, even kilowatt power level Nd:YAG lasers are available commercially; these have special applications in industrial processing [4]. With the recent development of high-power, high-heat capacity lasers, Nd:YAG has become a focus of current research. Compared with the widely used Nd:GGG crystal, the Nd:YAG crystal has advantages in its thermal and physical-chemical properties: For example, its thermal-lens effect is only one-half as much as that of Nd:GGG and lies below the thermal-stress limit; and its theoretical laser output is one-third higher [5].

A large-aperture, high-performance Nd:YAG crystal is the key material used in high-average-power solid-state lasers,

Table 1. Physical, chemical, and thermal properties of YAG.

Property	Detail	Concentration of Nd^{3+} (at.%)
Formula	$Y_3Al_5O_{12}$	—
Relative molecular mass	593.7	—
Mohr hardness	8–8.5	—
Melting point	1950 °C	—
Density	4.55 g·cm^{-3}	—
Thermal conductivity	0.14 W·cm^3·K^{-1}	0.725
Specific heat capacity	371.79 J·(mol·K)$^{-1}$	0.725
Thermal diffusivity	0.05 cm^2·s^{-1}	0.725
Thermal expansion coefficient	6.9×10^{-6} °C^{-1}	0.725
Refractive index	1.823	0.725
dn/dT	7.3×10^{-6} °C^{-1}	0.725
Dielectric constant	$\varepsilon_0 = 11.7$, $\varepsilon_\infty = 3.65$	0.725
Color	Pure YAG is colorless, and Nd^{3+}-doped YAG is purple	—
Optical homogeneity	Related to the crystal diameter with a general value of 0.2 in^{-1}	0.9
Chemical stability	Insoluble in sulfuric, phosphoric, nitric and hydrofluoric acid at room temperature; soluble in phosphoric acid at temperatures over 250 °C	—

and it has exhibited many unique and promising applications in the industrial, scientific, and military fields. In military technology, the development of high-power laser technology has led to significant changes in the field, and high-power solid-state lasers with an output power of 100 kW are particularly suitable for tactical laser weapons. The research and production of Nd:YAG crystals are mainly concentrated in the US and China. In the US, the II-VI and Northrop Grumman Synoptic companies focus on the production of Nd:YAG laser crystals, and the processing technology and quality achieved ranks at the leading level in the world. Convex-interface growth technology is used for crystal growth in the US; crystal diameters of 150 mm with a 250–300 mm length have been reached; an optical homogeneity value of 0.1λ per inch has been attained; and a variation in doping concentration of less than 10% has been achieved. In China, the Beijing Opto-Electronics Technology Co., Ltd. and Chengdu Dongjun Laser Co., Ltd. are the most well-known companies in this area. They also use the convex-interface growth technology for the commercial production of Nd:YAG crystals, and have achieved a diameter of 100 mm and a length of 200–230 mm. In addition, the Chengdu Dongjun Laser Co., Ltd. has developed a plane-interface technology for growing free "core" Nd:YAG crystals with a diameter of 50 mm and a length of 160 mm. Figure 1 shows the Nd:YAG crystal boule and a large Nd:YAG slab.

In the development of lasers, Yb-doped YAG (Yb:YAG) shows advantages in producing high-efficiency high-power lasers due to its high quantum-lasing efficiency. In fact, since the early 1990s, many internationally well-known research institutions have carried out studies on Yb:YAG crystals and the resulting lasers, which are assumed to be an important path toward developing high-power lasers [5–8]. In 1991, the Lincoln Laboratory at Massachusetts Institute of Technology (MIT) in the US first produced a Yb:YAG laser with an InGaAs laser diode as the pump source at a room-temperature output power of 12 mW. In 2004, an output power of 4.4 kW was real-
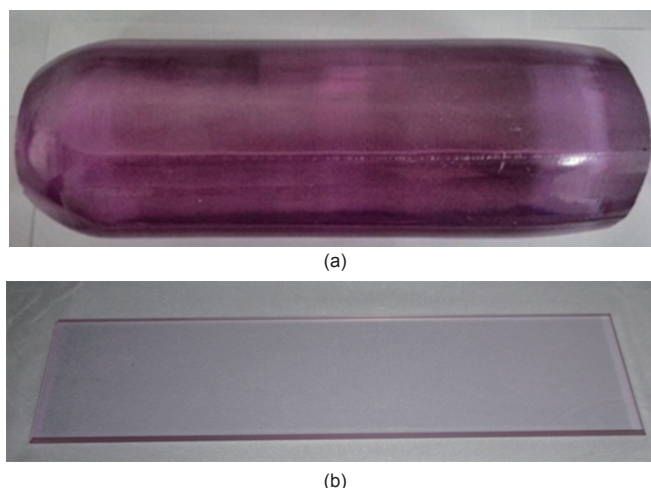

(a)

(b)

Figure 1. (a) Nd:YAG crystal boule; (b) Nd:YAG slab. Both were grown by Chengdu Dongjun Laser Co., Ltd.

ized in a Yb:YAG disc laser at the Hughes Research Laboratories, where an output power over 5 kW was recently obtained. In 2004, the German Trump company introduced a 4 kW Yb:YAG industrial disc laser and showed that a greater than 10 kW laser could be achieved with a single disc. In 2013, the Singapore National Laboratory operated a 1.1 kW single-disc Yb:YAG disc laser near the diffraction limit; this achievement represents the highest output power yet obtained in a single-disc laser [9]. In China, a 1 kW Yb:YAG laser was first realized at Tsinghua University. In addition to continuous-wave lasers, pulsed lasers with a pulse width of 136 fs and an output power of 3 W ranked as the shortest-pulse width lasers using Yb:YAG. In 2014, the Max-Planck Institute of Quantum Optics reported a maximum output power of 270 W with a peak power of 28 MW in a self-mode-locked Yb:YAG laser, which is the highest power for a mode-locked laser to date [10].

2.1.2 Titanium sapphire laser crystals

Titanium sapphire (Ti:Al_2O_3) has a broad wavelength band

and excellent thermal, optical, physical, and mechanical properties. Compared with the well-known Cr^{3+}:$BeAl_2O_4$, Cr^{3+}:LiCAF, and Cr:Mg_2SiO_4 laser crystals, Ti:Al_2O_3 has a much broader emission spectrum, ranging from 660 nm to 1200 nm. In theory, the shortest possible pulse width that can be achieved in Ti:Al_2O_3 is 3.3 fs, so Ti:Al_2O_3 is considered to be an ideal femtosecond ultrashort pulsed-laser crystal. In addition, it also serves as a high-power tunable and high-power ultrashort pulsed-laser medium for oscillation and amplification, and has promising applications in terawatt laser applications.

In 1982, Moulton first reported on a tunable pulsed Ti:Al_2O_3 laser. Since then, the Ti:Al_2O_3 crystal has attracted a great deal of attention from researchers. At present, the large size available for the Ti:Al_2O_3 crystal illustrates its importance in the PW laser and ultrafast high-energy laser driving systems [11–15] as a revolutionary material. Lawrence Livermore National Laboratory (LLNL) successfully demonstrated a 1.5 PW ultra-high-output power and 3×10^{20} W·cm^{-2} focused laser intensity with this crystal. In 2012, the Advanced Photonics Research Institute in Korea reported 1.5 PW lasers based on a Ti:Al_2O_3 laser crystal with a diameter of 100 mm [16]. In 2013, using a 100 mm diameter Ti:Al_2O_3 crystal, the Shanghai Institute of Optics and Fine Mechanics of Chinese Academy of Sciences (CAS) demonstrated a 2 PW Ti:Al_2O_3 laser, which is the highest peak-power obtained to date [15]. In order to increase the laser output power, the diameter of the Ti:Al_2O_3 laser crystal must be increased. For instance, for a 5–10 PW laser system, a crystal with a diameter of 200 mm is required. Therefore, the development of a high-quality Ti:Al_2O_3 laser crystal with a larger aperture has become an important research goal and would help to improve high-power ultrashort pulsed-laser systems [17–19].

Titanium sapphire crystal-growth methods include heat-exchange, Czochralski, Kyropoulos, and temperature-gradient techniques. In 2010, a high-quality Ti:Al_2O_3 crystal with a diameter of 208 mm was produced by the CSI company in the US using the heat-exchange method and devices with a diameter of 175 mm were produced [18]. In 2011, French scientists used the Kyropoulos method to grow a high-quality Ti:Al_2O_3 crystal with a diameter of 100 mm [19]. In China, the Shanghai Institute of Optics and Fine Mechanics has grown a ϕ120 mm × 80 mm Ti:Al_2O_3 crystal using the temperature-gradient method with a variation of the doping concentration ranging from 0.02 at.% to 0.52 at.%, a peak absorption coefficient at 490 nm of up to 9.0 cm^{-1}, and a figure of merit (FOM) value of up to 300, after high-temperature annealing [20]. In 2014, they used the heat-exchange method to grow a Ti:Al_2O_3 crystal with a diameter greater than 200 mm, and were able to produce a ϕ157 mm × 27 mm crystal, shown in Figure 2.

2.1.3 Rare earth sesquioxide laser crystals

Rare earth sesquioxide crystals (including Y_2O_3, Sc_2O_3, and Lu_2O_3) have a cubic structure and high thermal conductivity. The thermal conductivity of Y_2O_3 is 12.8 W·$(m\cdot K)^{-1}$ [21], while currently available high-power laser YAG crystals have values of 9.8 W·$(m\cdot K)^{-1}$ or 11 W·$(m\cdot K)^{-1}$ [22, 23]. In addition, Y_2O_3 has a low photon energy (less than 400 cm^{-1}, while YAG has a value of 700 cm^{-1}) [22, 23] and a high melting point
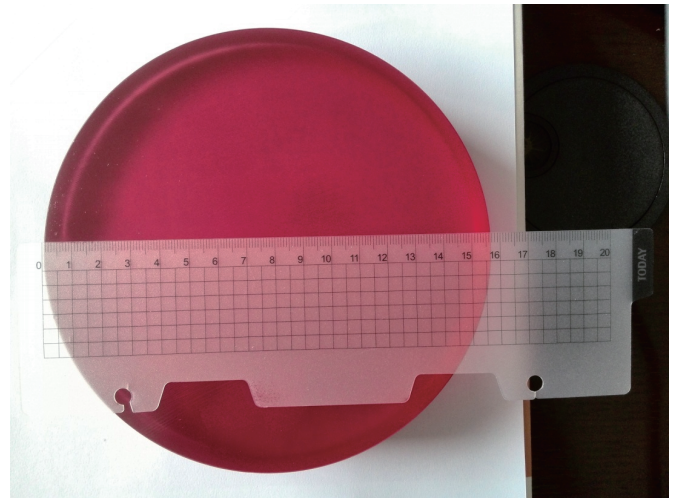

Figure 2. ϕ157 mm × 27 mm Ti:Al_2O_3 crystal grown by the Shanghai Institute of Optics and Fine Mechanics.

(above 2400 °C). These crystals are considered to hold promise for applications as high-power laser media. In 1964, Hoskins demonstrated stimulated emission in an Nd:Y_2O_3 crystal at low temperature [24]. However, an inability to attain excellent-quality sesquioxide crystals, because of their high melting temperatures, constrained their application. In 1999, based on improvements in crystal-growth techniques, Huber's team summarized the basic physical properties of sesquioxide laser crystals and, by comparison, those of YAG. They concluded that the sesquioxides have great advantages for use in high-power lasers [25]. In addition, the reported Nd:Sc_2O_3 laser output at 966 nm, 1.08 µm, and 1.49 µm shows potential for applications in radar and eye-safe laser systems [26]. The sesquioxides also provide a suitable internal crystalline field for Yb^{3+} ions [27]. In 2004, Klopp et al. first reported a femtosecond mode-locked Yb:Sc_2O_3 laser with a pulse width of 230 fs and an output power of 0.54 W [28]. In 2007, Petermann et al. reported the development of a Yb:Lu_2O_3 laser with a slope efficiency of 80%, an output power of 32.6 W, and a tunability range of 90 nm [21]. In 2009, Baer et al. demonstrated a Yb:Lu_2O_3 laser with an output power of 63 W and a pulse width of 535 fs. This laser also produced a continuous wave power of up to 149 W [29]. In 2010, Baer et al. improved the output power of the mode-locked Yb:Lu_2O_3 laser by producing a maximum output power of 141 W, a pulse width of 738 fs, and a peak power of 2.8 MW in the absence of amplification [30].

In 2011, based on previous reports on Lu_2O_3, Sc_2O_3, and Y_2O_3 that detailed aspects of their structure and growth habits, we synthesized polycrystalline materials designed to serve as sesquioxide laser crystals, and proposed that the optical floating zone method would be suitable for producing the high-melting-point sesquioxides, since this method is free of any crucible and can provide different atmospheres (Ar, N_2, or O_2) at high temperatures up to 3000 °C. By using a directional seed to initiate crystal growth and by using a suitable annealing technique, the quality of the crystals was improved and the crack-density problem was solved. At the present time, Nd-, Yb-, and Tm-doped Lu_2O_3 crystals have been produced. A crystal with Tm doping is shown in Figure 3.

Figure 3. A Tm:Lu$_2$O$_3$ crystal boule grown by the optical floating zone method.

Based on the availability of high-quality single crystals, the basic physical properties of Nd:Lu$_2$O$_3$ were investigated, including the crystal structure, the effective segregation coefficient, the thermal properties (thermal diffusivity, specific heat, and thermal conductivity), and the spectrum properties. Using Judd-Ofelt (J-O) theory, the spectrum parameters of the crystals were calculated and theoretically characterized. In Nd:Lu$_2$O$_3$ laser experiments, 0.143 W of continuous-wave laser output at 0.95 μm, and 2.81 W at dual wavelengths (1076 nm and 1080 nm) were demonstrated, which represent the highest output power to date in an Nd:Lu$_2$O$_3$ crystal laser [31]. In the near future, high-power laser performance will be studied.

2.1.4 Vanadate laser crystals with zircon structure

Vanadate crystals with a zircon structure are members of the tetragonal system and have the I4$_1$/amd space group. This class of crystals includes YVO$_4$ [32], GdVO$_4$ [33], LuVO$_4$ [34], ScVO$_4$ [35], and their mixed crystals [36, 37]. Since the 1990s, YVO$_4$ has become the most widely studied member of this group. Besides acting as a laser host material, YVO$_4$ is also a very good birefringent crystal with a birefringence of Δn = 0.2054–0.2225 in the range of 0.63–1.30 μm and in the transparent range from 0.45 μm to 4.8 μm. When doped with Nd^{3+} ions, it becomes a laser gain medium with a large polarized emission cross-section and an absorption coefficient consistent with the emission of commercial GaAlAs laser diodes. This compatibility provides a favorable situation for the design of high-efficiency lasers, and so Nd:YVO$_4$ has become an important laser material for the fabrication of laser-diode pumped solid-state lasers [32].

Because of its small thermal conductivity (~5 W·(m·K)$^{-1}$), its anisotropic physical properties (e.g., the thermal expansion coefficient, where a = 4.43 × 10^{-6} K^{-1} and c = 11.4 × 10^{-6} K^{-1}), and the reduction of V^{5+} ions into lower valence states under an anoxic atmosphere, crystal growth is difficult for YVO$_4$, and the grown crystal easily becomes darkened [38]. However, in an atmosphere containing oxygen, vanadium oxide is volatilized, which induces the accommodation of the melt components. Therefore, for a very long time, it has not been difficult

to obtain high optical-quality laser crystals of this material for laser applications [39, 40].

In the early 1990s, many new growth methods were invented, such as the optimized Czochralski method, the optical floating zone method, the laser-heated pedestal and the top-seeded method. As a result, large and high-quality vanadate crystals are available, as shown in Figure 4. The most widely used of these methods is the optimized Czochralski method [41]. The Nd:YVO$_4$ crystal has been widely used in moderate-power lasers; when combined with potassium titanyl phosphate (KTiOPO$_4$, or KTP) for frequency-doubling, it is also widely applied to the commercial production of low-power green lasers. In the high-power field, a continuous-wave Nd:YVO$_4$ laser with an output power of 110 W at 1.06 μm and an optical conversion efficiency of 44% was reported [42], and a laser with an output power of 43.6 W at 1.34 μm was reported [43]. With respect to pulsed lasers, EO actively Q-switched Nd:YVO$_4$ lasers were reported with pulse widths of 115 ps and 50 ps near the turn of the last century [44, 45]. In mode-locked Nd:YVO$_4$ lasers, an output power of 105 W was achieved with a pulse width of 8.4 ps [46].
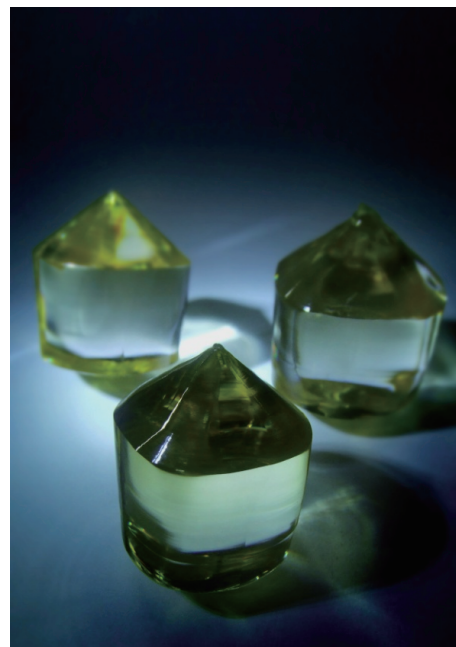

Figure 4. An Nd:YVO$_4$ crystal grown by the Czochralski method.

An Nd:GdVO$_4$ crystal was first successfully grown by Russian and German scientists [33]. It has a fluorescence lifetime of 90 μs and a large emission cross section (7.6 × 10^{-19} cm^2 at 1.06 μm). It should be noted that Nd:GdVO$_4$ has a thermal conductivity comparable with that of YAG (11.7 W·(m·K)$^{-1}$, which is twice the value for YVO$_4$ crystals). The reported spectrum and laser properties of Nd:GdVO$_4$ indicate that this crystal holds great promise in applications at moderate-power and even high-power levels. In 2002, an Nd:LuVO$_4$ crystal was reportedly grown by the flux method [34]. Nd:LuVO$_4$ has the largest emission cross-section (14.6 × 10^{-19} cm^2 at 1.06 μm) of all the vanadate crystals [34]. In 2003, we grew an Nd:LuVO$_4$ crystal with a large size and excellent quality by using the Czochral-

ski method [47, 48]. From that time on, Nd:LuVO$_4$ has been widely studied. In recent years, in order to broaden the absorption and emission spectra, mixed vanadate crystals have been developed and represent a series of suitable materials for constructing pulsed lasers due to their large inhomogeneous spectral broadening [36, 37].

2.1.5 Rare earth calcium oxygen borate laser crystals

This class of crystals includes YCa$_4$O(BO$_3$)$_3$ (YCOB), GdCa$_4$O(BO$_3$)$_3$ (GdCOB), and so forth, and belongs to the oxygen borate family with the space group Cm. With the Czochralski method, crystals of large size and high quality can readily be grown. In early studies on this series of crystals, the focus was placed on their applications as a nonlinear material with nonlinear coefficients comparable to those of β-BaB$_2$O$_4$ (BBO) and LiB$_3$O$_5$ (LBO) [49]. Large YCOB crystals can easily be grown and are considered to be excellent materials for frequency-doubling and third-harmonic generation at 1.06 mm [50–53]. When doped with Nd, Yb, or other active ions, they can be employed as a laser medium or as a self-frequency-doubling laser crystal [50]. In previous work, Ye et al. observed Nd:YCOB laser output with a Ti:Al$_2$O$_3$ laser as the pump source at a maximum output power of 404 mW with an absorbed power of 1 W [51]. Aka et al. grew an Nd:GdCOB crystal and developed an Nd:GdCOB laser with a slope efficiency of 34% with a Ti:Al$_2$O$_3$ laser as the pump source [54]. With a laser diode as the pump source, the output power of an Nd:YCOB laser reached 1.9 W at 1060 nm with a pump power of 3.7 W. Doped with Yb^{3+} ions, they become excellent tunable and mode-locked laser materials, since they have long fluorescence lifetimes and a suitable central absorption wavelength of 976 nm that matches the emission wavelength of InGaAs laser diodes. The highest continuous-wave power attained in a Yb:YCOB laser is currently 101 W when it is pumped with a laser diode [55]. The mode-locked pulse widths in Yb:YCOB and Yb:GdCOB are 35 fs and 90 fs, respectively [56].

In the self-frequency-doubling regime, it was found that the maximum nonlinear coefficients, d_{eff}, of YCOB and GdCOB occur along the direction out of the principal plane, and that they are about three times larger than those in the principal plane [57]. As shown in Figure 5, in comparison to the rare earth calcium oxygen borate crystals, Nd:GdCOB exhibits excellent overall performance and has many prospective practical applications. Based on optimal coupling between the fundamental lasing and the frequency-doubling effect, a maximum power of 3.01 W was attained in a self-frequency-doubling Nd:GdCOB laser [58]. It is suggested that the self-frequency-doubling Nd:GdCOB laser holds good promise for applications in laser displays and other low-power green laser products. At this point in time, self-frequency-doubling Nd:GdCOB crystals and lasers are well-commercialized.

2.2 NLO crystals

When light passes through an optical medium with a nonlinear polarization response, heterodyne wave generation occurs at the sum or difference frequency. This effect, which is dependent on the intensity of the laser light and which is different from linear light phenomena, is called the NLO effect.

Figure 5. An 8% Nd:GdCOB crystal boule.

Crystals that exhibit the NLO effect are called NLO crystals. Normally, a laser emits radiation at only one specific wavelength, but by using an NLO crystal, it is possible to obtain laser emission at different wavelengths [59, 60]. This technology is based on having a high-quality NLO crystal of suitable size and superb NLO properties.

In the late 1970s, a KTP crystal with excellent NLO properties was first developed by Du Pont, where it was grown by the hydrothermal method. This proved to be the best NLO crystal for operation in the visible to near-ultraviolet (UV) region. High-quality KTP crystals grown by the flux method, developed by Chinese scientists, opened a new era of wide application of these crystals in various fields at low cost. Since the 1980s, a series of Chinese-developed NLO crystals have been produced based on the anion-group theory developed by C. T. Chen and his colleagues, including BBO, LBO, and K$_2$Be$_2$BO$_3$F (KBBF) crystals. BBO and LBO have been widely used and commercialized since the late 1980s. KBBF is the only crystal that can be found in practical applications in the deep-UV (DUV) employing sixth-harmonic generation of the Nd-laser.

At present, research goals in this field involve looking for new crystals with even better quality, larger size, and superior NLO characteristics, especially in the DUV and in the mid- or far-IR regions of the spectrum, and even extended to THz frequencies for meeting the new requirements of emerging technologies. Other topics for the exploration of new crystals that have attracted more attention than ever before include Raman-shift and EO properties.

2.2.1 Lithium triborate crystals

Lithium triborate (LiB$_3$O$_5$, or LBO) crystals are mainly used for second- and third-harmonic generation in the operation of UV lasers. These crystals belong to the orthorhombic system, with point group (PG) C$_{2v}$-mm2, space group (SG) Pna2$_1$, a density of 2.47 g·cm^{-3}, and the following cell parameters: a = 0.84473 nm, b = 0.73788 nm, c = 0.51395 nm, and Z = 4. The structure contains groups (B$_3$O$_7$) that are the origin of the large nonlinearity. The emission range of LBO covers 160 nm –2.6 μm. As a negative biaxial crystal, it has a middle-of-the range birefringence value of about 10^{-6}. Type I and type II phase matching (PM) of the second and third harmonics can be achieved using Nd lasers. The effective NLO coefficient is

three times larger than the coefficient d_{36} in KDP. Noncritical PM can be realized by temperature tuning (T_{PM} = 112 °C). The LBO crystal possesses a high damage threshold, superior stability, non-deliquescence, and medium hardness (Mohr hardness of 6–7), affording easy cutting, grinding, and coating.

Large high-quality LBO crystals can be successfully grown with the flux method, an especially refined top-seeded solution-growth (TSSG) process that uses borate flux. This method is a new flux system, mainly containing K_2O-MoO_3 that was first used by Russian scientists, and which has been improved to enable the growth of large LBO crystals to be used in the manufacture of large second-harmonic genera-tion (SHG) and third-harmonic generation (THG) crystal devices in high-power output systems such as optical parametric chirped pulse amplification (OPCPA).

Before 2007, the largest LBO crystal produced weighed 570 g, as reported by Rus-sian scientists. In 2007, a crystal weighing 1116.8 g was produced by Hu's group [61, 62]. This was followed by the development of a crystal with the dimensions of 170 mm × 160 mm × 79 mm and a weight of 1596 g, which was grown in 90 days using an improved flux system [61, 62]. With these Li_2O-B_2O_3-MoO_3 systems, to-gether with the application of a rotating crucible and the use of a PM-oriented seed crystal, large LBO crystals have been produced; the weight of the largest LBO crys-tal that was recently obtained is more than 5000 g. A 50 mm × 50 mm sized SHG device was produced from this crystal. Recently, an even larger LBO device that is 80 mm on each edge was provided to the Shanghai Institute of Optics and Fine Me-chanics, CAS for OPCPA performance. A highest OPCPA output power of 0.61 PW was obtained with this device. In the near future, LBO devices larger than 200 mm in size will be produced, and progress will be made in advancing the techniques for growing large LBO crystals in order to meet the requirements of PW or even EW OPCPA laser outputs. Figure 6 shows one of the large LBO crystals.
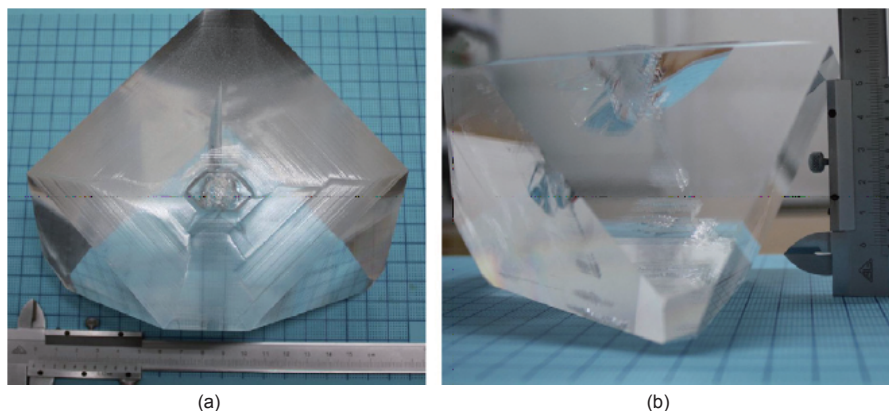

Figure 6. An LBO crystal grown by Hu's group with dimensions of 160 mm × 150 mm × 77 mm and a weight of 1988 g.

2.2.2 *β*-barium borate crystals
β-barium borate (*β*-BaB_2O_4, or BBO) is the low-temperature phase of BBO, and in the 1980s was the first Chinese-developed UV NLO crystal. It belongs to the trigonal system with PG C_{3v}-3m and SG R3C. The cell parameters are $a = b =$ 1.2532 nm, c = 1.2717 nm, $\alpha = \beta$ = 90°, γ = 120°, and Z = 6. The crystal density is 3.85 g·cm^{-3}, with a Mohr hardness of 4. The crystal consists of BO_3 planar groups that are the origin of the nonlinearity [63]. The transmission range of BBO, which is a negative mono-axial crystal with large birefringence, covers 189 nm–3.5 μm. The PM range for an Nd laser is 0.205–1.50 μm, and it can be used for SHG, THG, and fourth-harmonic generation (FHG). The shortest wavelength, 213 nm, can be obtained using BBO through SHG in a ruby, argon, or dye laser. The NLO coeffi-cient d_{11} is 4.1 times larger than the KDP coefficient d_{36}. It has superior mechanical properties, a high damage threshold, wide temperature acceptance, and large EO coefficients [63, 64].

The BBO crystal, shown in Figure 7, can be grown with flux or by TSSG methods. The selection of the flux is very important, and large high-quality transparent BBO crystals can be grown with a flux system containing mainly Na_2O or NaF [64].
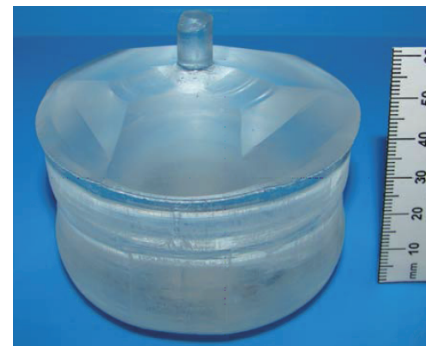

Figure 7. A BBO crystal, 55 mm in size and oriented along the *c*-axis, that was grown with NaF flux [64].

BBO crystals are mainly used to make frequency modulators, including frequency-doubling and optical pa-rameter oscillators. It is one of the most widely used UV NLO crystals, and has been commercialized as a high-tech product since the late 1980s. Chinese companies provide a large quantity of high-quality BBO crystals and devices worldwide.

2.2.3 Potassium fluoroboratoberyllate crystals
The potassium fluoroboratoberyllate ($K_2Be_2BO_3F$, or KBBF) crystal belongs to the trigonal system, PG 32, and has these cell parameters: a = 0.4472 nm and c = 1.8744 nm. It cleaves easily, and the cleavage progress is quite rapid along the [001] direction. The transmis-sion range runs from DUV at 155 nm to 3.7 μm, and the NLO coefficient d_{11} is 0.49 pm·V^{-1} at 1.0642 μm. Based on the anion-group theory, and through a long process of exploration combined with crystal engineering, chemical syn-thesis, structure determination, crystal growth, device design, and laser and device experiments, the discovery and successful application of the KBBF crys-tal broke the so-called DUV "walls." At this point in time, it is the only crystal that is suitable for practical use in the DUV-spectrum region.

Although KBBF has superior NLO

properties and is suitable for use in the DUV region, it is very difficult to grow because of its layered structure. By using spontaneous growth, a specially designed sealed crucible and corresponding furnace have been constructed. Using a flux system containing mainly KF and B_2O_3, a single KBBF crystal with the dimensions of 20 mm × 20 mm × 1.8 mm was first grown in 2001. In recent years, new crystal-growth technology has been developed, including local seed formation and high-temperature oscillation to control spontaneous seeding, resulting in the growth of large and thick KBBF crystals. The quality, area, and thickness of as-grown KBBF crystals have been greatly improved. The area of a high-quality KBBF crystal can be as large as 30 mm × 20 mm, with a thickness of 4 mm as shown in Figure 8(a). By contrast, the thickness of hydrothermally grown KBBF crystals can be larger than 6 mm along the *c*-axis, as shown in Figure 8(b) [65, 66], but the SHG efficiency for hydrothermally grown KBBF is one or two orders of magnitude smaller than that for flux-grown crystals. It was also found that SHG efficiency does not increase with increasing crystal thickness in the SHG PM orientation. The reason for this is due to the presence of the centered phase of KBBF in hydrothermally grown crystals, which strongly reduces the SHG efficiency.
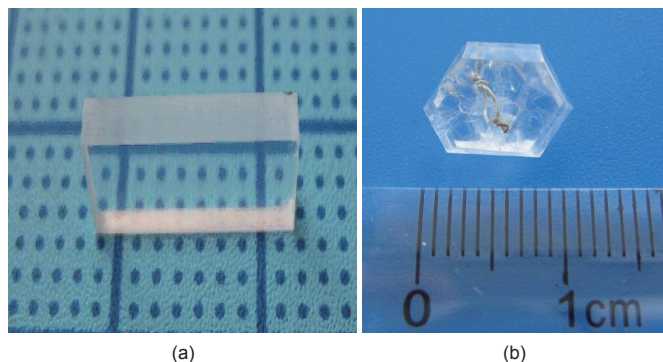

Figure 8. Potassium fluoroboratoberyllate crystal. (a) Flux grown; (b) hydrothermally grown [65].

Based on prism-coupling device (KBBF-PCD) technology, the difficulty of cutting the crystal along the PM orientation has been solved and highly efficient DUV laser output with good beam quality has been obtained. In 2003, the first reported sixth-harmonic generation in an Nd laser at 177.3 nm was achieved, and broke through the DUV "walls." In 2008, using a 14 mm × 6 mm × 2.1 mm KBBF crystal, the 177.3 nm output power of the $Nd:YVO_4$ sixth harmonic reached 12.95 mW, with an efficiency of 0.37% [67]; in the picosecond (ps) Nd:YAG laser system, the 177.3 nm sixth harmonic output power reached as high as 34.7 mW, with an efficiency of 0.82% [68]. The KBBF-PCD is stable for a long time with adequate cooling. Watt-level power output of the fourth harmonic in a Ti:sapphire laser was observed, and the output wavelength was found to be tunable over the spectral region from 185 nm to 200 nm [69]. In 2012, the mean power output of a ps-pulsed laser reached 41 mW, and the mean power output reached the 30 mW level in a nanosecond (ns)-pulsed laser. Wide spectral tuning of the FHG in the Ti:sapphire laser was also achieved in the range of 170–232.5 nm, and the fs 193.5 nm pulse power

reached 1.05 W. A continuous-wave output level of 1.3 mW at 191 nm with a narrow bandwidth of 150 kHz is significant for atomic or ion laser cooling, in the determination of the spectral parameters of hydrogen and anti-hydrogen. At this point in time, almost all kinds of DUV lasers, including ns-, ps-, and fs-pulsed, quasi-continuous-wave output, diode-pumped all-solid-state lasers have been developed. These lasers have enabled the manufacture of newly designed DUV research instruments, including high-resolution photo-electron energy spectrometers, spin- and angle-resolved photo-electron energy spectrometers, tunable phonon-energy DUV-laser photo-electron energy spectrometers, DUV-laser Raman spectrometers, and DUV-laser phonon-emitting electron micrometers. By using the newly developed photo-electron energy spectrometer, the superconducting bandgap was directly observed for the first time, providing new evidence to confirm the mechanism of superconductivity [70].

The NLO properties of KBBF arise mainly from the anion groups $(Be_2BO_3F_2)_{n\to\infty}$, $RbBe_2BO_3F_2$ (RBBF), and $CsBe_2BO_3F_2$ (CBBF), and were successfully obtained by cation replacement [71]. RBBF also belongs to the trigonal system with PG 32 and SG R32. There is a layered character in this crystal similar to KBBF along the *c*-axis. The thickness of the RBBF crystal is about 2 mm. The cutoff edge of the crystal is 160 nm, and the PM output should theoretically be 170 nm according to calculations. Using two RBBF-PCDs, a wide-range DUV tunable laser with output ranging from 175 nm to 232.5 nm was demonstrated, with power output greater than 1 mW. The maximum output power of 43.3 mW occurs at 202.5 nm. These results confirm that RBBF also has the potential to function as a DUV NLO crystal [72, 73]. A small CBBF crystal was grown with a UV cutoff of 150 nm.

2.2.4 Zinc germanium phosphor crystals

The mid-IR range is an important wavelength band that is used for applications such as laser radar, detection of carbon dioxide, detection of drugs, and laser targeting. Research on IR NLO crystals is one of the primary topics in NLO investigation.

Zinc germanium phosphorus ($ZnGeP_2$, or ZGP) is the best NLO crystal used for emission in 3–5 μm IR lasers, and is the key element in laser instruments in this range [74, 75]. Since the late 1980s, ZGP crystals have attracted much research interest due to urgent needs in industry, especially for military applications. Because phosphorus is volatile, the crystal is highly anisotropic in thermal expansion and has high absorption in the IR; therefore, the growth of large, high-quality ZGP crystals is a big challenge [76, 77].

Lei et al. have grown $\phi 50$ mm × 140 mm ZGP single crystals and produced a series of ZGP IR elements for IR optical parameter oscillators (OPOs) [78]. Laser output over the range of 3.8–4.5 μm was obtained when pumped with 2 μm input, and the laser output power can reach 30 W [78]. By using a 5.5 mm × 6.0 mm × 18.0 mm type I PM ($\theta = 55°$, $\varphi = 0°$) ZGP crystal, an OPO device was produced that exhibits a 10 mW output power over the range of 3–5 μm when pumped with a 5.2 W 2 μm laser. The O—O efficiency at 2 μm was 12%, and the repetition frequency was 4 kHz.

In this group, a series of new technologies has been developed for the growth of high-quality ZGP crystals. First, a horizontal dual-temperature zone furnace was designed for preparing stoichiometric ZGP polycrystalline material without germanium-rich composition. High-purity single-phase ZGP polycrystals up to 500 g can be repeatedly synthesized with this apparatus. Using the Bridgman method, large crack-free ZGP crystals up to ϕ50 mm × 140 mm in size were grown with a designed temperature field that resulted in a weakly concave interface, thereby effectively reducing the defect density. The absorption coefficient in the middle part of the grown crystal was reduced to a value as low as 0.01 cm^{-1}, which enables its use in 3–5 µm IR laser systems. Figure 9 shows the as-grown ZGP crystals and the IR elements produced from these crystals.
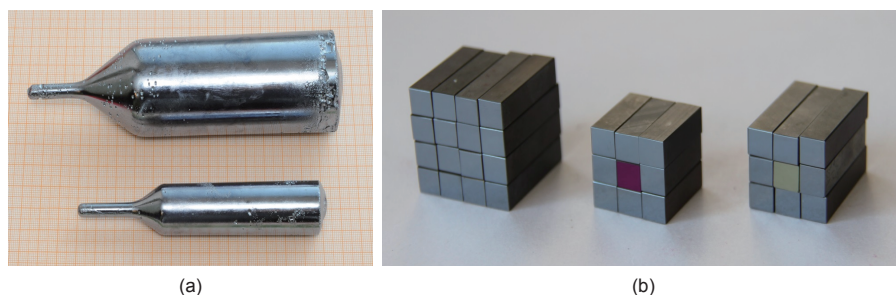

<center>(a)</center> <center>(b)</center>

Figure 9. ϕ50 mm × 140 mm ZGP crystals and IR elements.

2.2.5 Lithium indium sulfide and lithium indium selenide crystals

Lithium indium sulfide (LiInS$_2$, or LIS) is a new IR NLO crystal that was developed in recent years. It belongs to the orthorhombic system, with PG mm2, and the following cell parameters: a = 0.6890 nm, b = 0.8053 nm, and c = 0.6478 nm. The crystal has a density of 3.54 g·cm^{-3}, a Mohr hardness of 3–4, a transmittance range from 0.34 µm to 13.2 µm, and a thermal conductivity that was determined to be greater than 6 W·(m·K)$^{-1}$. The second-order NLO coefficients are: d_{31} = 7.2 pm·V^{-1}, d_{32} = 5.7 pm·V^{-1}, and d_{33} = –16 pm·V^{-1} (at 2.3 µm). The crystal was damaged when it was irradiated by a 100 MW·cm^{-2} pulsed laser at 1.064 µm (10 ns, 10 Hz). LIS is the only crystal in which Ti:sapphire laser emission at the wavelength of 5–11 µm can be frequency doubled. The crystal is normally grown with the Bridgman method, and it has a melting point of about 1000 °C.

Lithium indium selenide (LiInSe$_2$, or LISe) is the isotropic member of the LIS family. It also belongs to the orthorhombic system, and its cell parameters are: a = 0.71971 nm, b = 0.84116 nm, and c = 0.67926 nm. The transmittance range is 0.46–14 µm, the NLO coefficient d_{31} is 10.4 pm·V^{-1} (at 2.8 µm), and coefficient d_{32} is 7.8 pm·V^{-1} (at 2.1–2.45 µm). The thermal conductivity is five times as large as that of AgGaS$_2$ and the damage threshold is one or two orders of magnitude greater than those of most other IR NLO crystals.

LIS and LISe crystals were successfully grown with a modified Bridgman method by Tao's group at Shandong University [79]. By improving the temperature field, and using crucible rotation and a well-designed growth process, high-quality LIS crystals of up to ϕ16 mm × 50 mm in size were successfully grown. The size of as-grown LISe crystals reached as large as ϕ12 mm × 50 mm. Based on the crystals that were obtained, Sellmire equations for LIS were determined, and the PM curves for type II PM in the XY plane (θ = 90°) were obtained. The PM angle is calculated to be θ = 90° and φ = 55.5° for 1064 nm input radiation. A 1.536 µm and 3.47 µm IR laser can be obtained using this cut of the crystal through the difference frequency heterodyne process. The LIS crystal used was 3.5 mm × 3.5 mm × 4 mm in size. IR light was emitted from the crystal when pumped by 1064.2 nm and 1535.8 nm lasers, with an output energy of 80–100 µJ. The output frequency was the difference between the two incident lasers at 3.466 µm, and the efficiency was about 0.2%.

2.2.6 Barium tellurium molybdate crystals

Barium tellurium molybdate (BaTeMo$_2$O$_9$, or BTM) crystal is a newly developed oxide IR NLO crystal. It belongs to the monoclinic system, with PG P2. A transparent crystal sized 40 mm × 30 mm × 30 mm was grown with the flux method. The transmittance is 0.5 at 5.3 µm. The NLO coefficients are: d_{31} = 10.18 pm·V^{-1}, d_{24} = 3.64 pm·V^{-1}, and d_{15} = 1.91 pm·V^{-1}, as determined by Maker's method. The largest effective NLO coefficient in the main plane is d_{eff} = 10.36 pm·V^{-1}, and both type I and type II PM can be accomplished in the main frequency ranges. The crystal is stable with good physical and chemical properties. During the growth of BTM crystals, another phase was discovered. It is denoted as α-BaTeMo$_2$O$_9$ (α-BTM), and belongs to the orthorhombic system, with PG mm2, and SG Pca2$_1$. Its cell parameters are: a = 14.8683(2) Å, b = 5.66360(10) Å, c = 17.6849(3) Å, and Z = 8. Compared with β-BTM, the NLO coefficient of α-BTM is about 1/12 as great, that is, 0.2 times the KDP coefficient d_{36}. Pure phases of β-BTM or α-BTM can be synthesized at temperatures of 550 °C and 590 °C, respectively. With an increase in temperature, for example, from 550 °C to 570 °C, pure phase β-BTM is partially converted to α-BTM. At 585 °C, along with an increase in reaction time, pure phase α-BTM can be obtained by the transition of β-BTM, with BaMoO$_4$ and amorphous tellurium. However, pure phase β-BTM cannot be fully converted to α-BTM through heating without the addition of BaMoO$_4$. It appears that the addition of BaMoO$_4$ reduces the energy barrier for phase transition [80].

Using a β-BaTeMo$_2$O$_9$ crystal of 20 mm in size, oriented along the Z-direction, a stimulated Raman-shift laser at 921 cm^{-1} and 905.7 cm^{-1} was produced when pumped with a 1064 nm laser. The output power of the first-order Raman laser reached 1.9 W, and with a 35 mm α-BTM crystal, the O—O efficiency was 31.5%.

2.2.7 Growth of NLO crystals used in THz-band and laser performances

The THz wavelength laser is very im-

portant and useful. Topics for this subject are focused on the manufacture of THz sources. Among these, the production of NLO crystals that can be used in this band is very important. Normally, various organic single crystals are the candidates for operation at these wavelengths.

2.2.8 DAST crystals

DAST is an organic ionic NLO crystal. The formula for the crystal is $C_{23}H_{26}N_2O_3S$; that is, 4-N,N-dimethylamino-4′-N′-methyl-stilbazolium tosylate, abbreviated as DAST. It belongs to the monoclinic system, with PG m and SG Cc. Its cell parameters are: a = 10.365 Å, b = 11.322 Å, c = 17.893 Å, α = 90°, β = 92.24°, γ = 90°, and Z = 4. It has large NLO coefficient values: d_{11}(1318 nm) = 1010 pm·V^{-1}, d_{11}(1542 nm) = 290 pm·V^{-1}, and d_{26}(1542 nm) = 39 pm·V^{-1}. The EO coefficients are also large: r_{11}(720 nm) = 92 pm·V^{-1}, r_{11}(1313 nm) = 53 pm·V^{-1}, and r_{11}(1535 nm) = 47 pm·V^{-1}. The melting point of DAST is about 256 °C. High-quality DAST crystals of 10 mm × 10 mm × 2 mm in size can be grown with the slow-cooling method in solution (Figure 10). The quality of the crystals was assessed using X-ray rocking curves on the [001] facet. PM for THz generation occurs in the range of 720–1650 nm, and efficient THz generation and detection is possible in the range of 0.3–16 THz (Figure 11). The maximum output energy measured was 0.75 nJ at 2.71 THz, and the efficiency approached 10^{-6}.
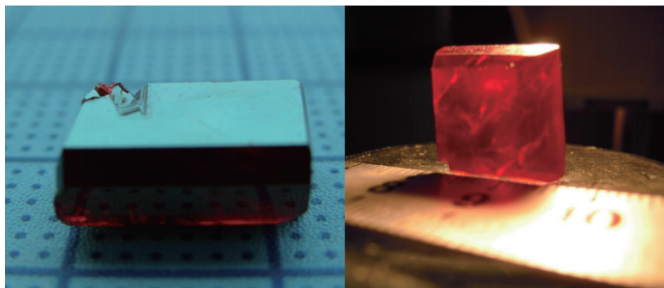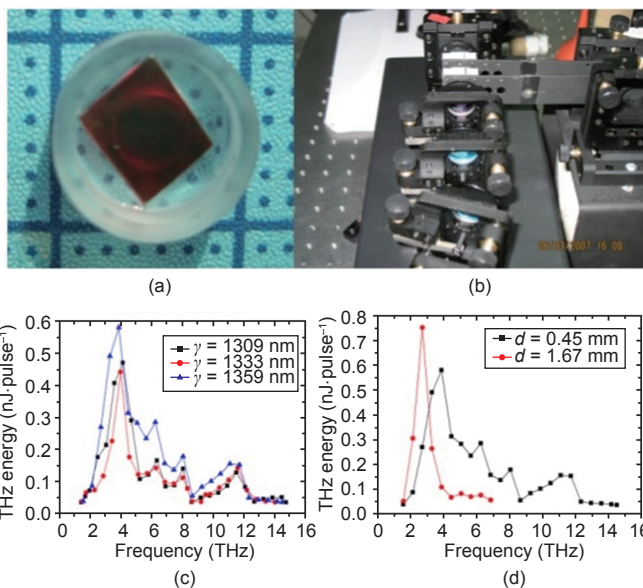

Figure 10. DAST as-grown crystals.

Figure 11. THz radiation obtained from a DAST crystal [81].

2.2.9 DSTMS crystals

DSTMS has the chemical formula $C_{25}H_{30}N_2O_3S$ and the full chemical name 4-N,N-dimethylamino-4′-N′-methyl-stilbazolium 2,4,6-tri-methylbenzenesulfonate. This crystal belongs to the monoclinic system, with PG m and SG Cc. Its cell parameters are: a = 10.266 Å, b = 12.279 Å, c = 17.963 Å, α = 90°, β = 93.04°, γ = 90°, and Z = 4. The crystal was grown by the slow-cooling method with methanol selected as the solvent. The starting temperature was 45 °C with a cooling rate of 0.3 °C per day, a DSTMS crystal of 10 mm × 10 mm × 1 mm in size was grown over six days. The melting temperature was determined to be 257.8 °C, and the decomposition temperature determined to be 327.3 °C by thermal analysis. From the NLO difference frequency process, tunable THz radiation was obtained over the range of 0.88–19.27 THz. The maximum output power was 85.3 nJ (at 3.80 THz), the corresponding peak output power was 17.9 W, and the efficiency was 3.6% [81].

2.2.10 OH1 crystals

OH1 has the chemical formula $C_{19}H_{18}N_2O$ and the chemical name 2-(3-(4-hydroxystyryl)-5,5-dimethylcyclohex-2-enylidene) malononitrile. This crystal belongs to the orthorhombic system, with PG mm2 and SG Pna2$_1$. The cell parameters are: a = 15.4408 Å, b = 10.9939 Å, c = 9.5709 Å, α = β = γ = 90°, and Z = 4. The NLO coefficient d_{33} is 120 pm·V^{-1}. Although it is an organic crystal, it does not dissolve in water and possesses no hydrated form. It can serve as an alternative for DAST in THz wave generation. Centimeter-sized OH1 crystals have been grown with the slow-cooling method from a methanol solution. The starting temperature was 43 °C with a cooling rate of 0.5 °C per day. Using a bulk seed crystal, a high-quality OH1 octahedral single crystal with the dimensions of 11 mm × 11 mm × 10 mm was grown and is shown in Figure 12 [82]. X-ray rocking-curve measurements confirmed its quality. Indentation measurements determined the hardness on the [100] and [111] faces to be 0.67 GPa and 0.5 GPa, respectively. Transmission in the range of 800–1400 nm was about 60%, and 40%–70% in the range of 1400–2600 nm, with several absorption peaks. A transparency window exists from 4 μm to 6 μm. By means of optical rectification, tunable narrow-band 0.83–3.13 THz wave output was produced using a Ti:shappire laser. The optimum pump-laser wavelength is around 1350 nm. For THz generation near the 1 THz band, OH1 is obviously superior to DAST [83].

2.2.11 BaGa$_4$S$_7$ and BaGa$_4$Se$_7$ crystals

BaGa$_4$S$_7$ and BaGa$_4$Se$_7$ are two recently investigated chalcogenide crystals that can potentially be used in the mid- and far-IR bands. BaGa$_4$S$_7$ (abbreviated as BGS) belongs to the orthorhombic system with PG mm2 and SG Pna2$_1$. The transmission range of BGS covers 350 nm to 13.7 μm. The structure of this crystal was determined in 1983 and Ye et al. has grown BGS with a length of 30 mm and a diameter of 12 in using the Bridgman method and also determined its NLO properties, especially for IR applications [84]. The results showed that the NLO coefficient is about 1.2 times as large as in a LiInS$_2$ crystal grown by the powder SHG method. Under irradiation from a 1.064 μm pulsed laser (pulse width of 15 ns), the damage
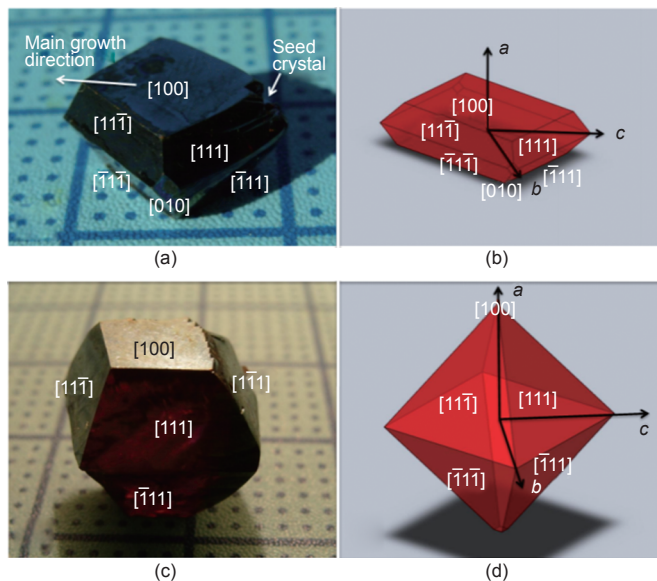
Figure 12. An OH1 as-grown crystal [82].

threshold was measured to be 105 MW·cm⁻² and 4.3 MW·cm⁻² in the range of 3–5 μm. Based on a determination of the refractive indices, calculations showed that the OPO PM wavelength lies in the range of 3–5 μm, and noncritical OPO PM can be achieved at 9.6 μm under 2 μm pumping. This is the only crystal that can support noncritical PM in this band. The NLO coefficients of BGS are d_{31} = 5.1 pm·V⁻¹ and d_{22} = 5.7 pm·V⁻¹.

BaGa$_4$Se$_7$ (BGSe) is an analog crystal of BGS, but belongs to the monoclinic system, with PG m and SG Pc. Single-crystal BGSe can be grown with the Bridgman method. The structure of BGSe has been determined, and it is believed that it is more stable, and that its nonlinearity is larger than that of BGS on account of its structure [85]. Investigation into the IR properties and the possible applications of BGSe is in progress.

2.3 EO crystals

The EO effect is a phenomenon in which the refractive index changes with an applied electric field. The situation where the refractive index changes is proportional to the external electric field; this property is called the linear EO or Pockels effect. The case where the refractive index change is proportional to the square of the external electric field is called the secondary EO Kerr effect. Although the change in the refractive index of the crystal caused by the EO effect is generally small, it is sufficient to change the light propagation in the crystal. By modulating the external electric field, the interacting optical and electrical signals are controlled, modulated, and transformed by each other.

Since the invention of the laser in the 1960s, the occurrence of any EO crystal that possesses excellent comprehensive performance is rare. For a long time, the only practical EO crystals available were potassium dideuterium phosphate (KD$_2$PO$_4$, or KDP) and lithium niobate (LiNbO$_3$, or LN). In recent years, some newer EO crystals, barium metaborate (β-BaB$_2$O$_4$, or BBO) and rubidium titanyl phosphate (Rb-TiOPO$_4$, or RTP), were developed. Currently, the available EO crystals can fully meet the basic requirements for light

modulators and laser devices. The rapid development of laser and optical communications techniques requires novel EO crystals and devices.

Current research on EO crystals must rely on the models of NLO crystals that have been developed. Based on these models, the development of new EO crystals starts with an analysis of the microscopic structure, followed by a determination of the structure and the symmetry groups that favor a large EO effect. Based on macroscopic symmetry, the possible PGs of EO crystals can be found, and by considering interaction and composition effects, the development of EO crystals with optical activity has recently become possible. Research on the above effects is still in progress and has achieved some results.

Historically, an excellent EO crystal is also a favorable choice for use as a Q-switch. BBO was the first representative Chinese crystal, discovered by Chinese scientists in 1985. This crystal belongs to the trigonal system with PG 3m, a translucent band width (189 nm–3.5 μm), and a linear EO coefficient $γ_{22}$ of 2.2 pm·V⁻¹. The size of the crystal was 6 mm × 6 mm × 20 mm, with a half-wave voltage $V_{λ/4}$ of 7.7 kV, and an optical damage threshold value of 50 GW·cm⁻² at 1064 nm. Transverse effects used in generating EO Q-switching are especially suitable for high-power-density solid-state lasers. BBO is an excellent EO crystal and can be used for EO Q-switching in pulsed lasers with high-average power and a high-repetition rate [86]. However, it is still difficult to grow high-quality crystals with a large length along the Z-direction. Although BBO crystals with a length of over 200 mm have been grown, the cost is still quite high, which constrains many extensive applications to lasers. Goodno et al. have reduced the half-wavelength voltage of BBO by using the technique of reducing the cross-sectional area of the crystal [87]. With a 6 mm × 6 mm × 20 mm BBO crystal as an EO Q-switch, Stolzenburg et al. obtained a green laser output power of 102 W at 515 nm by using a 7 mm long type I phase-matching LBO crystal for frequency-doubling in a Yb:YAG microchip laser [88].

Potassium titanyl phosphate (KTiOPO$_4$, or KTP) and rubidium titanyl phosphate (RbTiOPO$_4$, or RTP) are excellent NLO and EO crystals. Having been developed in China by means of the flux method, they have become the commercial materials of choice for frequency-doubling. KTP and RTP belong to the orthorhombic system with PG mm2. The transmission bands range in 0.35–4.5 μm (KTP) and 0.35–5.1 μm (RTP), and the EO coefficients are as follows: $γ_{23}$ is 15.7 pm·V⁻¹ (KTP) and 17.5 pm·V⁻¹ (RTP), and $γ_{33}$ is 36.3 pm·V⁻¹ (KTP) and 40.5 pm·V⁻¹ (RTP). KTP is subject to easy breakdown when a high-intensity electric field is applied, and gray tracks appear. The RTP crystal has low conductivity in the Z-direction, a high optical-damage threshold, and no tendency to produce gray tracks. As a result, RTP has become a commercial EO Q-switch. In recent years, there have been many reports and articles on the production and application of KTP and RTP crystals as EO Q-switches, especially regarding high-quality KTP and RTP crystals grown in Israel. In 2001, Roth reported the growth of a KTP crystal for EO applications using the top-seeded flux method [89]. In 2005, he reported a series of

RTP crystals grown using the top-seeded method but with different [Rb]/[P] atomic ratios (1.25–2) in a self-flux system with different solute concentrations (0.55–1.1 g RTP/g flux). He showed that RTP crystals are similar to KTP crystals, with a close stoichiometric ratio to the chemical groups in the flux [90]. In 2008, Tseitlin et al. reported the growth of high-impedance RTP crystals, and obtained a mono-domain RTP crystal up to 330 g in weight [91]. By using faster-pulling and slower-cooling techniques, the crystal exhibited an almost constant [100] cross-section. It is suitable for application as an EO switch, since RTP can withstand a high-intensity electric field [91]. In 2010, Roth and Tseitlin summarized their crystal-growth techniques for obtaining large, high-optical quality RTP crystals [92]. Depending on the requirements of the EO switch, $K_6P_4O_{13}$ or $Rb_4P_4O_{13}$ solvents can respectively grow high-quality KTP and RTP crystals. Also, the addition of PbO in the solvent can reduce the viscosity, increasing the solubility and thereby reducing the oxygen vacancy density, which is helpful for avoiding the generation of gray tracks. Because of the changes in the natural birefringence caused by temperature variation, two RTP crystal devices with the same dimensions but rotated by 90° must be used to compensate for the phase change caused by temperature variation.

Langasite ($La_3Ga_5SiO_{14}$, or LGS) is a type of crystal that exhibits laser, piezoelectric, and EO properties. A grown LGS crystal is shown in Figure 13. From crystal physics, if a crystal possesses piezoelectric properties, it also has EO and NLO properties; and crystals with PG 32 symmetry exhibit optical activity. In the applications of EO Q-switching, optical activity rotates the polarization plane of the incident light and complicates the design of an EO switch. LGS belongs to PG 32 and has a UV-absorption edge at 242 nm with optical activity. Using the interferometry method, the EO coefficients of LGS crystals were determined to be γ_{11} = 2.3 pm·V^{-1} and γ_{41} = 1.8 pm·V^{-1}. When LGS is used for EO Q-switching using transverse EO effects, the half-wave voltage V_n is about 17 000 V at λ = 1.064 µm with an aspect ratio l/d = 1:1; therefore, an aspect ratio between 4:1–5:1, such as with dimensions of 10 mm × 10 mm × 40 mm ($X \times Y \times Z$), causes the half-wave voltage to drop to 3000–4000 V. Measured under the same conditions, the damage threshold of DKDP, LGS, and LiNbO$_3$ crystals are 260 MW·cm^{-2}, 950 MW·cm^{-2}, and 100 MW·cm^{-2}, respectively [93]. LGS EO Q-switches are based on transverse EO properties and are designed as follows: The crystal is cut along the Z-direction, and the EO field is applied along the X-direction. Comparison experiments between LGS and DKDP that have been performed showed that the Q-switching performance is comparable with an insertion loss of 1.92% and an output energy of up to 359 mJ under a pump energy of 520 mJ. With the development of high-quality LGS crystals and EO Q-switching technology, LGS Q-switched lasers with high power output and high repetition rate have been developed. In high repetition-rate Q-switched lasers, the highest frequency that can be reached is 50 kHz with a maximum output power of 7.5 W, and a pulse width of 46 ns. Using a double end-pumped design, the laser output power can be further increased to 12.5 W. Considering the high-optical damage threshold, the LGS crystal has excellent promise for

application in EO Q-switching. In addition to applications in the near-IR range, in 2012, Wang et al. extended coverage of the LGS EO switch to 2.09 µm [94] and 2.79 µm [95] lasers with a pulse energy of 520 mJ and 216 mJ, respectively.
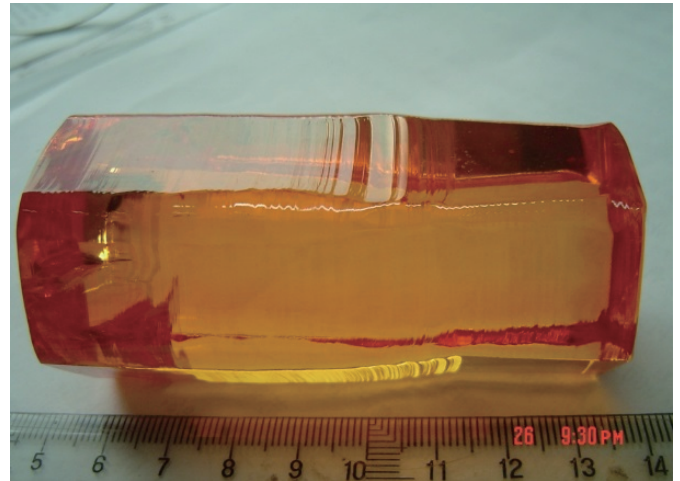

Figure 13. A langasite optical crystal grown at Shandong University.

2.4 Scintillation crystals

A crystal that emits luminescent light (scintillation) when it is exposed to high-energy radiation is called a scintillation crystal. Scintillation crystals can be used to detect different kinds of radiation, so they are widely applied in nuclear medicine, high-energy physics (e.g., electron positron collider), nuclear physics, space physics, geological exploration, the detection of explosives, and other industries. Inorganic scintillation crystals are important because they possess the advantages of high density, stability, and superior scintillation properties. Typical scintillation crystals include: bismuth germanate ($Bi_4Ge_3O_{12}$, or BGO), lead tungstate (PbWO$_4$, or PWO), sodium iodide (NaI:Tl), cesium iodide (CsI:Tl), barium fluoride (BaF$_2$), and ytterbium aluminate (YAlO$_3$:Ce). The establishment of large-scale particle accelerators promoted the large-scale application of scintillation crystals throughout the world. The invention of and wide application of X-ray computed tomography (X-CT) and positron-emission tomography (PET) have made the scintillation crystal one of the major types of functional crystals, with high commercial profits. With advances in nuclear diagnosis and nuclear medicine, the development of scintillation crystals has entered into a new era. The needs of molecular medical imaging technology, experimental high-energy physics, and radiation detection under extreme conditions have promoted the exploration and investigation of new scintillation crystals with high luminescent efficiency, high resolution, quick response time, and high radiation-damage threshold. During the past thirty years, a series of high-quality scintillation crystals made in China were provided to many large international facilities. Some examples include the BGO crystal used in the L3 experiment, the PWO used in the Large Hadron Collider (LHC) of the European Organization for Nuclear Research (CERN), and the CsI(Cl) used in the Belle experiment in Japan (KEK) and in the BaBar experiment at the Stanford Linear Accelera-

tor Collider (SLAC) in the US.

BGO is an excellent scintillation crystal that emits green fluorescence light at a peak wavelength of 480 nm. Due to a high effective atomic number and high density, BGO is a very efficient γ-ray absorber and has been used where high stopping power is required, especially for the detection of high-energy γ-rays. Due to its high radiation hardness, high scintillation efficiency, good energy resolution, and lack of hygroscopicity, the BGO scintillation crystal has been proven to be reliable in oil and gas well logging for many years. BGO is used in nuclear medicine, typically in computed tomography (CT), and in experimental high-energy physics such as the L3 experiment at CERN, for which around 12 tons of BGO was used. These experiments mark a milestone in the development of Chinese functional-crystal production as a contribution to progress in international engineering and science. At this point in time, BGO scintillation crystals are fully commercialized in China. For example, high-quality cut and polished monolithic pixilated BGO crystals of cylindrical shape with a diameter of 76 mm and a length of 300 mm, or with rectangular shape and the dimensions of 40 mm × 80 mm × 200 mm, are available for specific applications (Figure 14).

Figure 14. (a) BGO and (b) PWO crystals used in high-energy physics facilities.

The decay time for BGO is, however, relatively long and the cost of raw materials is relatively expensive. Bismuth silicate ($Bi_4Si_3O_{12}$, or BSO) is a new scintillation crystal with excellent mechanical properties, good chemical stability, and quick response. It has the potential to serve as an alternative replacement crystal for BGO. Now, moreover, so-called the third-generation scintillators with the formula RE_2SiO_5, where R is a rare earth element, have been found to possess excellent scintillation properties, including Lu_2SiO_5 (LSO), Gd_2SiO_5 (GSO), and Y_2SiO_5 (YSO).

The PWO crystal (Figure 14) has a high density (8.28 g·cm^{-3}), high effective atomic number ($Z_{eff} = 73$), and a fast decay time (6/30 ns). This crystal has the shortest radiation-length and Moliere-radius values at 0.9 cm and 2.19 cm, respectively, and radiation damage only appears at doses exceeding 105 Gy. Although the light output of the $PbWO_4$ scintillator is as low as about 0.5% of that of the NaI:Tl scintillator, it was found to be quite suitable for incorporation into the Electromagnetic CALorimeter (ECAL), the photon detector of the CMS and ALICE experiments at CERN. It was also selected as the basic material to build the ECAL of the BTeV experiment at the Fermi National Accelerator Laboratory in the US. Considering its high density and fast decay time, it may also have prospects for extensive application in nuclear medical diagnostics.

$CdWO_4$ (CWO) is another good scintillation crystal that has a high density (7.90 g·cm^{-3}), short radiation length (1.06 cm), high luminescence efficiency and resolution, large X-ray absorption, and high damage threshold, and is an excellent material for the manufacture of scintillation detectors, especially at low temperatures. Due to the volatility of the precursor composition component CdO, a high-quality CWO crystal is difficult to grow. Recently, on the basis of improvements in crystal-growth technology, a ϕ40 mm × 70 mm crystal was grown using the Bridgman method, and is available for use in a number of applications. CWO was selected as the detection material for heavy particles existing in the cosmos, an experiment that is aimed at proving the existence of weak mutual effects of particles (WIMP) [96]. Zinc tungstate ($ZnWO_4$) has a high density and high luminescence efficiency, and a good potential for detecting α, β, and 2β decay as well as dark mass [97]. Crystals of zinc tungstate larger than ϕ50 mm × 100 mm can be grown by the Bridgman method.

Aluminate crystals, including LuAP:Ce, GdAP:Ce, YAG:Ce, and YAP:Ce exhibit high temperature stability and can be used in oil exploration and other high-temperature applications. YAP:Ce is a new scintillation crystal with a high light yield (four times that of BGO), and a short decay time of less than 27 ns. Its density is 5.4 g·cm^{-3}. Its main luminescence peak appears at 366 nm, which is a good match for photoelectric detector requirements. It is effective for detecting γ-rays and soft X-rays due to its low effective atomic number ($Z_{eff} = 39$). YAP:Ce crystals larger than ϕ100 mm can be grown by pulling from the melt [98] and by using the temperature-gradient method. They have been used in γ-ray and soft X-ray detection, positron emission tomography (PET), and computed tomography, partly replacing CsI:Tl and BGO crystals.

In recent years, some new scintillation crystals have been developed, such as $Ce:Lu_{1.6}Y_{0.4}SiO_5$ (Ce:LYSO) and $LaBr_3$. LYSO has the advantages of high light output and density, quick decay time, and excellent energy resolution. These properties make LYSO an ideal candidate for a range of radiation-detection applications in nuclear physics and nuclear medicine, which require higher, improved timing resolution, and superior energy resolution. Crystals of dimensions of ϕ60 mm × 110 mm were grown with the pulling method. These crystals are available for use as γ-ray and X-ray detectors in such applications as PET, well logging, and high-energy physics, all of which require excellent coating capability. Different assembly

arrays can also be provided on request. Table 2 is a comparison of the properties of BGO and LYSO crystals.

Table 2. Comparison of the properties of BGO and LYSO crystals.

Properties	BGO	LYSO
Density (g·cm⁻³)	7.13	7.3
Melting point (°C)	1050	2047
Index of refraction	2.15	1.82
Radiation length (cm)	1.10	1.16
Attenuation (cm⁻¹)	0.96	0.87
Decay constant (ns)	300	50
Light yield (%) NaI (Nl)	25	75
Photofraction (%)	40	30
Energy resolution (511 keV, %)	16	20
Radioactivity	No	Yes

Another new scintillation crystal is cerium-doped lanthanum bromide ($Ce:LaBr_3$). This crystal belongs to the hexagonal system with SG $P6_3/m$, and a melting point of 772 °C. The crystal has a high light yield of 60 000 photons·MeV⁻¹ and a short decay time of 20 ns, together with a high energy resolution of about 3%. The combination of these superior properties has attracted much attention from researchers. This crystal can be used for the nondestructive detection of different kinds of radiation, especially those used in the anti-terrorism field. High-quality $Ce:LaBr_3$ crystals have been grown with the modified Bridgman method using a quartz crucible under completely dry conditions [99]. The temperature stability of the detection device that employs $Ce:LaBr_3$ is sufficiently good for the change in resolution to be less than ± 5% between –10 °C and 50 °C [100].

2.5 Relaxor ferroelectric single crystals

As one of the most important classes of electrically interactive materials, ferroelectric/piezoelectric crystals play key roles in the fabrication of precision actuators, sensors, transducers, and resonators. They have been widely used in fields, such as information technology, advanced manufacturing, resource and environment conservation, medical diagnostics, aerospace and astronautics, and defense applications. Scientists worldwide have been exerting great efforts to find new ferroelectric/piezoelectric materials to meet the rapid advancement in the application of electric devices [101, 102].

The relaxor ferroelectric $Pb(Mg_{1/3}Nb_{2/3})O_3$ (PMN) was discovered by Smolensky in the 1960s [103]. The relaxor ferroelectric single crystals $Pb(Zn_{1/3}Nb_{2/3})O_3$-$PbTiO_3$ (PZN-PT or PZNT) and $Pb(Mg_{1/3}Nb_{2/3})O_3$-$PbTiO_3$ (PMN-PT or PMNT) were grown from PbO flux by Park and Shrout in 1997 [104]. It was found that these two kinds of crystal exhibit good ultrahigh energy-density piezoelectric properties, with $d_{33} > 2000$ pC·N⁻¹ and $k_{33} \approx 92\%$, values that are much higher than those of conventional lead zirconate titanate ceramics ($d_{33} \approx 600$ pC·N⁻¹ and $k_{33} \approx 70\%$) [105]. This discovery was seen as an exciting breakthrough in a field that is over 50 years old and considered to be mature [106]. These exciting results have attracted considerable attention in the ferroelectric field. The US Navy (ONR) granted a total of about $100 million USD for

projects pertaining to the growth of PMNT single crystals and their device applications. Relaxor ferroelectric crystals have been used in EO and photo-sonic detectors in the IR region in recent years due to their superior properties [107–111]. The combination of different effects opens up an opportunity to develop multi-functional materials and devices [112, 113].

Over the past 10 years, a great deal of progress has been made in the growth of relaxor ferroelectric single crystals and in their applications in China, especially at the Shanghai Institute of Ceramics, CAS. The research is mainly aimed at growing crystals of large size and high quality to replace conventional piezoelectric transducer (PZT) ceramics for the next generation of high-performance electric devices, such as ultrasonic transducers and sensors.

It is difficult to grow complex crystals such as $(1–x)Pb(B_1B_2)O_3$-$xPbTiO_3$ (where B_1 = Mg^{2+}, Zn^{2+}, Ni^{2+}, In^{3+}, Sc^{3+} and B_2 = Nb^{5+}, Ta^{5+}, W^{6+}) because of phase instability at high temperature and associated pyrochlore phases that appear during crystal growth. On the basis of an investigation of the phase stability of PZNT and PMNT at high temperatures, it was found that the stable perovskite phase of the PZNT system can only exist in flux at high temperature. However, PMNT can be grown from its melt because its perovskite phase is quite stable at high temperature. The high-temperature phase diagram and the mechanism of crystal growth were investigated, and a modified technique was developed to grow large, high-quality PMNT single crystals, in which a seed crystal was introduced to control spontaneous nucleation and the associated pyrochlore phases.

Based on this research, large, high-quality PMNT single crystals up to a size of ϕ80 mm × 200 mm were grown directly from the melt by using the modified Bridgman method. This accomplishment has resulted in a breakthrough in the bottleneck of growing relaxor ferroelectric single crystals, since these crystals had previously been grown from the flux. The as-grown crystals are provided for research and for the manufacture of various devices and apparatuses. At the present time, this method is the only one available in the world for the practical growth of large relaxor ferroelectric single crystals.

The electrical and mechanical properties of PMNT are very different from those of PZNT ceramic. Much work has been done to explore the origin of its ultrahigh energy-density piezoelectric properties, so that the properties of the crystal can be optimized for practical applications. In addition, extra-high response pyroelectric and EO properties were found in PMNT crystals. After optimizing the comprehensive properties of these crystals, novel ultrasonic transducers, magneto-electric (ME) sensors, and IR detectors were designed and fabricated. These accomplishments serve to promote the applications of relaxor ferroelectric crystals for the next generation of electric devices.

Using measurements obtained with a polarizing light microscope, the monoclinic phase was observed in the composition range of 30%–35% PT content in PMNT single crystals. By cross-checking the dielectric/piezoelectric properties and by using X-ray diffraction (XRD) analysis, the composition ranges were verified where the rhombohedral, tetragonal,

monoclinic, and orthorhombic phases exist. The phase diagram of the PMNT system at low temperature was reported in the literature. An irreversible polarization rotation path that follows R↔M_A→M_C↔T was observed with an applied electric field along the [001] direction in rhombohedral PMNT single crystals at compositions near the morphotropic phase boundary (MPB), and the stable monoclinic phase was verified as monoclinic M_C. The peculiar polarization rotation path under an applied electric field is considered to be the origin of the ultrahigh energy-density piezoelectric coefficient. That is, the ultrahigh energy-density piezoelectric coefficient, which can reach up to 2500 pC·N^{-1} in [001]-oriented PMNT single crystals at compositions near the rhombohedral side of the MPB, results from the irreversible R↔M_A→M_C↔T polarization rotation path. The monoclinic phase acts as a bridge between the rhombohedral and tetragonal phases in relaxor ferroelectric single crystals at compositions near the MPB, and reveals the structural origin of the ultrahigh energy-density piezoelectric response in [001]-oriented rhombohedral PMNT single crystals.

The effects of the solid-solution composition and the structure of relaxor crystals on the phase-transition temperature and the dielectric and piezoelectric properties were measured. By adding Pb(In$_{1/2}$Nb$_{1/2}$)O$_3$ (PIN), the properties of PMNT can effectively be modified. Large, high-Curie-temperature Pb(In$_{1/2}$Nb$_{1/2}$)O$_3$-Pb(Mg$_{1/3}$Nb$_{2/3}$)O$_3$-PbTiO$_3$ (PIN-PMN-PT or PIMNT) crystals have been grown. While retaining the ultrahigh energy-density piezoelectric properties, the Curie temperature ($T_c \geqslant$ 190 °C), phase-transition temperature ($T_{rt} \geqslant$ 110 °C), and coercive field ($E_c \approx$ 520 V·mm^{-1}) were enhanced in the PIMNT crystal. Compared with PMNT, the values of T_c and T_{rt} of the PIMNT crystal are increased by 50 °C and 40 °C, respectively, and E_c is enhanced by a factor of two.

The dielectric loss in Mn-doped PMNT (Mn:PMNT) is reduced from 0.3% in the as-grown condition to 0.05% after doping at 1 kHz. By extended X-ray absorption fine-structure (EXAFS) analysis, the mechanism for significant reduction of the dielectric loss was observed in Mn:PMNT. This crystal greatly reduces the noise level that results from dielectric loss in IR and magnetic sensors, effectively enhancing the sensor detectivity.

An ultrahigh response pyroelectric coefficient of up to 15.3 × 10^{-4} Cm^{-2}·K^{-1} has been discovered in the PMN-26%PT crystal, a value that is four times higher than that of PZT ceramic. The pyroelectric coefficient decreases with PT content due to the diminished size of the ferroelectric domains, and the maximum pyroelectric coefficient and minimum permittivity occur along the orientation of spontaneous polarization. The figure of merit for detectivity of the Mn:PMN-26%PT crystal was found to be drastically increased from 15.3 × 10^{-5} Pa$^{-1/2}$ to 40.2 × 10^{-5} Pa$^{-1/2}$, much higher than the values for other pyroelectric materials (i.e., 12.6 × 10^{-5} Pa$^{-1/2}$ for LT crystal and 1.17 × 10^{-5} Pa$^{-1/2}$ for PZT ceramic). This creates a new application for the Mn:PMNT crystal in novel uncooled IR detectors.

The excellent linear EO effect (Pockels effect) and second-order EO effect (Kerr effect) performance of the PMNT crystal were also recently discovered. A PMN-33%PT crystal at the MPB composition exhibits a highest effective linear EO coefficient of 182 pm·V^{-1} (with a low half-wave voltage of 202 V), which is an order of magnitude higher than that of conventional LiNbO$_3$ crystals. The largest effective second-order EO coefficient (r_{11}-r_{12}) was observed in the composition range of $x \leqslant$ 0.08 in PMN-xPT crystals, which is at a value of 8.19 × 10^{-16} m^2·V^{-2} and which is much larger than the corresponding value of 2.8 × 10^{-16} m^2·V^{-2} in Pb$_{1-y}$La$_y$Zr$_{1-x}$Ti$_x$O$_3$ (PLZT) ceramics. The results show that the PMNT crystal is a promising candidate for next-generation EO devices, such as optical switches and optical attenuators for high-speed optical communications.

Because of the excellent magnetic properties of the PMNT crystal, a heterostructure ME composite with a piezoelectric transformer was designed and fabricated, in which the measured ME voltage coefficient reached as high as 57.3 V·Oe^{-1}, a value that is 50 times greater than that of conventional ME composites. The sensitivity of the ME sensor for detecting an alternating magnetic field was below 7 pT·Hz$^{-1/2}$ at 1 Hz. A PMNT-based 64-element phased-array ultrasonic transducer has been fabricated with a bandwidth about 20% higher than that of PZT transducers. An Mn:PMNT pyroelectric IR sensor has been fabricated with a detectivity of 2.2 × 10^9 cm·Hz$^{1/2}$·W^{-1}, a value that is three times higher than that of LiTaO$_3$ IR sensors. These results suggest the increasing application of relaxor ferroelectric crystals in the next generation of ME sensors, ultrasonic transducers, and pyroelectric IR detectors.

With regard to future work, high T_c and T_{rt} relaxor ferroelectric crystals represent the research emphasis in the field. For example, xPb(Mg$_{1/3}$Nb$_{2/3}$)O$_3$-yPb(In$_{1/2}$Nb$_{1/2}$)O$_3$-zPbTiO$_3$ (PIMNT), which has high T_c and T_{rt} (T_c > 180 °C, T_{rt} > 110 °C), is an excellent candidate for high-sensitivity and high-energy-density piezoelectric transducers [114]. A series of new relaxor ferroelectric crystals with three or four components is currently under investigation.

2.6 SiC crystals

The wide application of the first- and second-generation semiconductor crystals represented by silicon (Si) and gallium arsenate (GaAs) encouraged the rapid development of the microelectronic and photonic industries. However, most semiconductor devices constructed of Si or GaAs can be used only at temperatures below 200 °C. SiC is a crystal with many different polytypes. Generally speaking, there are two basic SiC types. One is β-SiC, which has cubic symmetry and is formed at a temperature of about 1600 °C. The other is α-SiC, which has hexagonal symmetry and is composed of more than a hundred different polytypes such as 4H, 15R, 6H, and so forth. At high temperature, β-SiC can slowly be transformed to α-SiC. 4H SiC forms at a temperature of 2000 °C, while 15R and 4H-SiC can be grown at a temperature above 2100 °C. At 2200 °C, the 6H SiC crystal is also stable, so it is widely used in industry.

SiC is a good substrate for laser diodes (LDs) and light-emitting diodes (LEDs), because the lattice parameters of SiC fully match those of GaN. However, the development of sapphire for GaN single crystals has somewhat hindered the application of SiC in the optical industry because of its high

cost compared with sapphire. It has a wide application in the electronics and electrical industries for manufacturing high-temperature devices, because it has a wide band gap (3 times that of Si), a high thermal conductivity (3.3 times that of Si and 10 times that of GaAs), a large mobility (2.5 times that of Si) and a high damage threshold field (10 times that of Si and 5 times that of GaAs).

In the past 20 years, China has developed SiC crystal-growth technology and related research on high-temperature devices that utilize SiC. At present, high-quality SiC crystals of up to 6 inches (150 mm) in diameter (Figure 15) can be successfully grown with the PVD method at Chinese facilities.

Figure 15. SiC crystal with a diameter of 6 inches (150 mm), grown by the Institute of Physics, CAS.

SiC single crystals with diameters up to 4 in and epi-ready wafers are available and have been commercialized in China. The reduction of defects, especially micropipe defects, is very important before SiC can be used in most applications. In 2009, Gao et al. reported that micropipes can be eliminated by using a well-designed temperature field and a modified growth procedure. Other defects, such as dislocations and low angle boundaries along [1–100] can also be reduced by reducing the temperature field in 6H-SiC single crystals grown by the sublimation method [115].

By using a SiC substrate, high-quality GaN/AlGaN HEMT devices were manufactured with a 2DEG mobility of 1800 cm^2·(Vs)$^{-1}$ and an output power of 5.5 W·mm^{-1}.

3 Discussion and conclusion

The application of functional crystals, and particularly photonic crystals, is related to the development of the all-solid-state laser. Currently, the development of glass, optical fiber, ceramic, laser diodes, liquid crystals, and nano-materials are challenging the utilization and application of many traditional functional crystals. The most important type of functional crystal is the semiconductor crystal, with Si as the most representative example. Si has played a key role in the modern information era, and has been found suitable for new applications, such as in the solar-energy industry.

As a photonic functional crystal, it also plays an important role in different fields, especially when used as a key material in the high-tech industry. The need for large, high-quality crystals promotes the development of crystal-growth technology. The main trends in the functional-crystal field

are directed toward the production of multi-functional, low-dimensional crystals designed to be part of devices that meet the requirements of all-solid-state lasers for extended wavelength, higher frequencies, shorter pulses, higher damage threshold and operation under extreme conditions.

Laser crystals with high quality, large size, and high thermal conductivity have attracted much attention and can emit laser radiation in new wavelength bands. In relation to the applications of DUV crystals, research on NLO crystals focuses on the development of crystals that can be operated from the IR down to the THz band. New scintillation, piezoelectric, ferroelectric, EO and other functional crystals are also of great interest in international science and technological research.

Since the 1980s, a new series of NLO crystals have been engineered and commercialized, opening a large-scale range of applications and a strong market. More recently, the successful application of scintillation crystals strengthened the situation. In the last few years, high-quality laser crystals and self-frequency-doubling crystals have been grown and widely used, continuing the development of functional crystals. The creation of ferroelectric PMNT and related crystals is also a milestone in the field. In the future, we will do our best to develop new functional crystals based on fundamental research on the relationship between structure and properties, and to develop a crystal engineering model to design new high-performance functional crystals. New crystal-growth technology and facilities are also key factors for the further development of functional crystals. Crystal growth is not a single process, but rather a combination of the preparation of raw materials, the treatment of the as-grown crystal, the cutting and polishing of the crystal, and the manufacture of devices. Thus, with the goal of extending the applications of crystals, one must pay attention to each step in the process in order to optimize the essential factors that result in high-quality crystals for practical use. The characterization and evaluation of functional crystals are pre-conditions for assessing the suitability for a given application, so we intend to develop a variety of effective methods and facilities to support the work.

Stemming from research on the relationship between crystal structure and crystal properties, and in order to develop a theory to accurately model material design, we intend to develop functional crystals with known properties, including crystals for advanced lasers as well as NLO, EO, scintillation, relaxation-ferroelectric, multifunctional, and substrate crystals. Our goal is to develop new methods and apparatuses for growing large, high-quality crystals, combined with basic research on crystal-growth mechanisms and related theories. It is essential to pay more attention to the areas related to crystal growth, such as the preparation of raw materials, crystal processing, and the application of coatings. To this end, one can contribute to the enhancement of the manufacture of crystal devices and apparatus that use functional crystals, in order to meet the needs of high-tech industry and defense. Another important goal is to combine functional crystals with semiconductor crystals, in applications that save energy and reduce carbon output.

In the near future, we will focus on the following topics:

(1) The relationship between crystal structures and crystal properties, and the origin of functional properties;

(2) The design and computer simulation of functional crystals;

(3) Growth dynamics and the process of crystal growth;

(4) The relationship between quality and the functional properties of a crystal and growth conditions, defect density, and possible applications; and

(5) The relationship between crystal symmetry and crystal properties of the multifunctional crystal and the combination of functional properties.

On the basis of the projected basic research listed above, more functional crystals with high quality and superior properties should become available in coming years.

Acknowledgements

Compliance with ethics guidelines

Jiyang Wang, Haohai Yu, Yicheng Wu, and Robert Boughton declare that they have no conflict of interest or financial conflicts to disclose.

References

1. T. H. Maiman. Stimulated optical radiation in ruby. *Nature*, 1960, 187(4736): 493–494

2. W. Koechner. *Solid-State Lasers Engineering*. W. Sun, Z. W. Jiang, G. X. Cheng, trans. Beijing: Science Press, 2002 (in Chinese)

3. J. E. Geusic, H. M. Marcos, L. G. Van Uitert. Laser oscillations in Nd-doped yttrium aluminum, yttrium gallium and gadolinium garnets. *Appl. Phys. Lett.*, 1964, 4(10): 182–184

4. A. Kruusing. Underwater and water-assisted laser processing: Part 2—Etching, cutting and rarely used methods. *Opt. Lasers Eng.*, 2004, 41(2): 329–352

5. B. Jiang, Z. Zhao, G. Zhao, J. Xu. Thin disk solid state lasers and heat capacity solid state lasers. *Laser & Optoelectronics Progress*, 2006, 43(3): 3–8 (in Chinese)

6. A. Heller. Efficiently changing the color of laser light. *S&TR*, 2006-10-19. https://str.llnl.gov/str/Oct06/Ebbers.html

7. H. Yin, P. Deng, F. Gan. Defects in YAG:Yb crystals. *J. Appl. Phys.*, 1998, 83(7): 3825–3828

8. J. Dong, A. Shirakawa, K. Ueda, J. Xu, P. Deng. Efficient laser oscillation of Yb:$Y_3Al_5O_{12}$ single crystal grown by temperature gradient technique. *Appl. Phys. Lett.*, 2006, 88(16): 161115

9. Y. H. Peng, Y. X. Lim, J. Cheng, Y. Guo, Y. Y. Cheah, K. S. Lai. Near fundamental mode 1.1 kW Yb:YAG thin-disk laser. *Opt. Lett.*, 2013, 38(10): 1709–1711

10. J. Brons, et al. Energy scaling of Kerr-lens mode-locked thin-disk oscillators. *Opt. Lett.*, 2014, 39(22): 6442–6445.

11. X. Liang, et al. Parasitic lasing suppression in high gain femtosecond petawatt Ti:sapphire amplifier. *Opt. Express*, 2007, 15(23): 15335–15341

12. V. Yanovsky, et al. Ultra-high intensity-300-TW laser at 0.1 Hz repetition rate. *Opt. Express*, 2008, 16(3): 2109–2114

13. Z. Wang, C. Liu, Z. Shen, Q. Zhang, H. Teng, Z. Wei. High-contrast 1.16 PW Ti:sapphire laser system combined with a doubled chirped-pulse amplification scheme and a femtosecond optical-parametric amplifier. *Opt. Lett.*, 2011, 36(16): 3194–3196

14. T. J. Yu, S. K. Lee, J. H. Sung, J. W. Yoon, T. M. Jeong, J. Lee. Generation of high-contrast, 30 fs, 1.5 PW laser pulses from chirped-pulse amplification Ti:sapphire laser. *Opt. Express*, 2012, 20(10): 10807–10815

15. Y. Chu, et al. High-contrast 2.0 Petawatt Ti:sapphire laser system. *Opt. Express*, 2013, 21(24): 29231–29239

16. V. Chvykov, K. Krushelnick. Large aperture multi-pass amplifiers for high peak power lasers. *Opt. Commun.*, 2012, 285(8): 2134–2136

17. H. Kiriyama, et al. Temporal contrast enhancement of petawatt-class laser pulses. *Opt. Lett.*, 2012, 37(16): 3363–3365

18. D. B. Joyce, F. Schmid. Progress in the growth of large scale Ti:sapphire crystals by the heat exchanger method (HEM) for petawatt class lasers. *J. Cryst. Growth*, 2010, 312(8): 1138–1141

19. A. Nehari, et al. Ti-doped sapphire (Al_2O_3) single crystals grown by the Kyropoulos technique and optical characterizations. *Cryst. Growth Des.*, 2011, 11(2): 445–448

20. S. F. Shao, et al. Research progress in numerical simulation for crystal growth by czochralski method. *J. Synth. Cryst.*, 2005, 34(4): 687–692 (in Chinese)

21. R. Peters, C. Kränkel, K. Petermann, G. Huber. Broadly tunable high-power Yb:Lu_2O_3 thin disk laser with 80% slope efficiency. *Opt. Express*, 2007, 15(11): 7075–7082

22. N. S. Prasad, et al. Recent progress in the development of neodymium-doped ceramic yttria. *IEEE J. Sel. Top. Quant.*, 2007, 13(3): 831–837

23. G. Boulon, et al. Search of optimized trivalent ytterbium doped-inorganic crystals for laser applications. *J. Alloy. Compd.*, 2002, 341(1–2): 2–7

24. R. H. Hoskins, B. H. Soffer. Stimulated emission from Y_2O_3:Nd^{3+}. *Appl. Phys. Lett.*, 1964, 4(1): 22–23

25. L. Fornasiero, E. Mix, V. Peters, E. Heumann, K. Petermann, G. Huber. Efficient laser operation of Nd:Sc_2O_3 at 966 nm, 1082 nm and 1486 nm. In: *OSA Trends in Optics and Photonics Vol.26 Advanced Solid-State lasers (Optical Society of America, 1999)*. Boston, MA, US, 1999: 249–251

26. L. Fornasiero, E. Mix, V. Peters, K. Petermann, G. Huber. New oxide crystals for solid state lasers. *Cryst. Res. Technol.*, 1999, 34(2): 255–260

27. K. Petermann, et al. Highly Yb-doped oxides for thin-disc lasers. *J. Cryst. Growth*, 2005, 275(1–2): 135–140

28. P. Klopp, V. Petrov, U. Griebner, K. Petermann, V. Peters, G. Erbert. Highly efficient mode-locked Yb:Sc_2O_3 laser. *Opt. Lett.*, 2004, 29(4): 391–393

29. C. R. E. Baer, et al. Femtosecond Yb:Lu_2O_3 thin disk laser with 63 W of average power. *Opt. Lett.*, 2009, 34(18): 2823–2825

30. C. R. E. Baer, et al. Femtosecond thin-disk laser with 141 W of average power. *Opt. Lett.*, 2010, 35(13): 2302–2304

31. L. Hao, et al. Spectroscopy and laser performance of Nd:Lu_2O_3 crystal. *Opt. Express*, 2011, 19(18): 17774–17779

32. J. R. O'Conner. Unusual crystal-field energy levels and efficient laser properties of YVO_4:Nd. *Appl. Phys. Lett.*, 1966, 9(11): 407–409

33. P. A. Studenikin, A. I. Zagumennyi, Y. D. Zavartsev, P. A. Popov, I. A. Shcherbakov. $GdVO_4$ as a new medium for solid-state lasers: Some optical and thermal properties of crystals doped with Cd^{3+}, Tm^{3+}, and Er^{3+} ions. *Quantum Electron.*, 1995, 25(12): 1162–1165

34. C. Maunier, J. L. Doualan, R. Moncorgé, A. Speghini, M. Bettinelli, E. Cavalli. Growth, spectroscopic characterization, and laser performance of

Nd:LuVO₄, a new infrared laser material that is suitable for diode pumping. *J. Opt. Soc. Am. B*, 2002, 19(8): 1794–1800

35. B. Yao, et al. Crystal growth and laser performance of neodymium-doped scandium orthovanadate. *J. Cryst. Growth*, 2010, 312(5): 720–723

36. J. Liu, et al. Pulse energy enhancement in passive *Q*-switching operation with a class of Nd:Gd$_x$Y$_{1-x}$VO₄ crystals. *Appl. Phys. Lett.*, 2003, 83(7): 1289–1291

37. H. Yu, et al. Enhancement of passive *Q*-switching performance with mixed Nd:Lu$_x$Gd$_{1-x}$VO₄ laser crystals. *Opt. Lett.*, 2007, 32(15): 2152–2154

38. P. P. Yaney, L. G. DeShazer. Spectroscopic studies and analysis of the laser states of Nd³⁺ in YVO₄. *J. Opt. Soc. Am.*, 1976, 66(12): 1405–1414

39. W. Li, E. Shi, W. Zhong, Z. Yin. Anion coordination polyhedron growth unit theory mode and crystal morphology. *J. Synth. Cryst.*, 1999, 28(2): 117–125 (in Chinese)

40. M. Wei, G. Li, Y. Zhu, X. Wu, Z. Yu, S. Teng. Raw material synthesis of yttrium vanadate crystals (Nd³⁺:YVO₄:YVO₄). *J. Synth. Cryst.*, 1998, 27(2): 178–181 (in Chinese)

41. X. Meng, L. Zhu, H. Zhang, C. Wang, Y. T. Chow, M. Lu. Growth, morphology and laser performance of Nd:YVO₄ crystal. *J. Cryst. Growth*, 1999, 200(1–2): 199–203

42. P. Shi, D. Li, H. Zhang, Y. Wang, K. Du. An 110 W Nd:YVO₄ slab laser with high beam quality output. *Opt. Commun.*, 2004, 229(1–6): 349–354

43. L. Cui, et al. 880 nm laser-diode end-pumped Nd:YVO₄ slab laser at 1342 nm. *Laser Phys.*, 2011, 21(1): 105–107

44. J. J. Zayhowski, C. Dill Iii. Coupled-cavity electro-optically *Q*-switched Nd:YVO₄ microchip lasers. *Opt. Lett.*, 1995, 20(7): 716–718

45. D. Nodop, J. Limpert, R. Hohmuth, W. Richter, M. Guina, A. Tünnermann. High-pulse-energy passively *Q*-switched quasi-monolithic microchip lasers operating in the sub-100-ps pulse regime. *Opt. Lett.*, 2007, 32(15): 2115–2117

46. H. Lin, J. Li, X. Liang. 105 W, <10 ps, TEM₀₀ laser output based on an in-band pumped Nd:YVO₄ Innoslab amplifier. *Opt. Lett.*, 2012, 37(13): 2634–2636

47. H. Zhang, et al. Growth of new laser crystal Nd:LuVO₄ by the Czochralski method. *J. Cryst. Growth*, 2003, 256(3–4): 292–297

48. J. Liu, et al. Continuous-wave and pulsed laser performance of Nd:LuVO₄ crystal. *Opt. Lett.*, 2004, 29(2): 168–170

49. W. K. Jang, Q. Ye, J. Eichenholz, M. C. Richardson, B. H. T. Chai. Second harmonic generation in Yb doped YCa₄O(BO₃)₃. *Opt. Commun.*, 1998, 155(4–6): 332–334

50. D. Vivien, F. Mongel, G. Aka, A. Kahn-Harari, D. Pelenc. Neodymium-activated Ca₄GdB₃O₁₀ (Nd:GdCOB): A multifunctional material exhibiting both laser and nonlinear optical properties. *Laser Phys.*, 1998, 8(3): 759–763

51. Q. Ye, B. H. T. Chai. Crystal growth of YCa₄O(BO₃)₃ and its orientation. *J. Cryst. Growth*, 1999, 197(1–2): 228–235

52. Z. Wang, K. Fu, X. Xu, X. Sun, H. Jiang, R. Song, J. Liu, J. Wang, Y. Liu, J. Wei, Z. Shao. The optimum configuration for the third-harmonic generation of 1.064 μm in a YCOB crystal. *Appl. Phys. B*, 2001, 72(7): 839–842

53. P. Yuan, G. Xie, D. Zhang, H. Zhong, L. Qian. High-contrast near-IR short pulses generated by a mid-IR optical parametric chirped-pulse amplifier with frequency doubling. *Opt. Lett.*, 2010, 35 (11): 1878–1880

54. G. Aka, et al. Linear- and nonlinear-optical properties of a new gadolinium calcium oxoborate crystal, Ca₄GdO(BO₃)₃. *J. Opt. Soc. Am. B*, 1997, 14(9): 2238–2247

55. O. H. Heckl, et al. Continuous-wave and modelocked Yb:YCOB thin disk laser: First demonstration and future prospects. *Opt. Express*, 2010, 18(18): 19201–19208

56. A. Yoshida, et al. Diode-pumped mode-locked Yb:YCOB laser generating

57. J. Y. Wang, H. H. Yu, H. J. Zhang, J. Li, N. Zong, Z. Y. Xu. Progress on the research and potential applications of self-frequency doubling crystals. *Progress in Phys.*, 2011, 31(2): 91–110 (in Chinese)

58. H. Yu, et al. Efficient high-power self-frequency-doubling Nd:GdCOB laser at 545 and 530 nm. *Opt. Lett.*, 2011, 36(19): 3852–3854

59. T. Hahn. *The International Tables for Crystallography.* Myrtle Beach, SC: Springer Press, 1983

60. G. Zhang, G. Lan, Y. Wang. *Lattice Vibrational Spectroscopy.* Beijing: Higher Education Press, 2001 (in Chinese)

61. Z. Hu, Y. Zhao. A method and its apparatus for the large size nonlinear optical crystal growth by combination of crucible and seed crystal: CN, 101503819. 2009-08-12 (in Chinese)

62. C. Chen, B. Wu, A. Jiang, G. You. A new type of ultraviolet SHG crystsl—β-BaB₂O₄. *Sci. Sin. Ser. B*, 1985, 28(4): 235–243

63. D. N. Nikogosyan. Beta barium borate (BBO). *Appl. Phys. A-Mater*, 1991, 52(6): 359–368

64. D. Perlov, S. Livneh, P. Czechowicz, A. Goldgirsh, D. Loiacono. Progress in growth of large β-BaB₂O₄ single crystals. *Cryst. Res. Technol.*, 2011, 46(7): 651–654

65. N. Ye, D. Tang. Hydrothermal growth of KBe₂BO₃F₂ crystals. *J. Cryst. Growth*, 2006, 293(2): 233–235

66. C. T. Chen. Recent advances in deep and vacuum-UV harmonic generation with KBBF crystal. *Opt. Mater.*, 2004**:** 26(4), 425–429

67. G. Wang, et al. 12.95 mW sixth harmonic generation with KBe₂BO₃F₂ crystal. *Appl. Phys. B-Lasers. O.*, 2008, 91(1): 95–97

68. C. T. Chen, G. L. Wang, X. Y. Wang, Z. Y. Xu. Deep-UV nonlinear optical crystal KBe₂BO₃F₂—Discovery, growth, optical properties and applications. *Appl. Phys. B-Lasers. O.*, 2009, 97(1): 9–25

69. T. Kanai, X. Wang, S. Adachi, S. Watanabe, C. Chen. Watt-level tunable deep ultraviolet light source by a KBBF prism-coupled device. *Opt Express*, 2009, 17(10): 8696–8703

70. G. Liu, et al. Development of a vacuum ultraviolet laser-based angle-resolved photoemission system with a superhigh energy resolution better than 1 meV. *Rev. Sci. Instrum.*, 2008, 79(2): 023105

71. X. Wen. *Theoretical and Experimental Study of Electrically Driven Traveling-Wave Thermoacoustic Refrigerator in Room Temperature Range.* Beijing: Technical Institute of Physics and Chemistry, CAS, 2006 (in Chinese)

72. C. Chen, et al. Deep UV nonlinear optical crystal: RbBe₂(BO₃)F₂. *J. Opt. Soc. Am. B*, 2009, 26(8): 1519–1525

73. H. Dai, C. Chen. Realization methods of laser jamming in helicopter with mid-infrared lasers. *Jour. Sichuan Ordnance*, 2011, 32(1): 114–116 (in Chinese)

74. D. Sandy. *Electronic Warfare Handbook 2008.* Berkshire: The Shephard Press Ltd., 2008

75. G. A. Verozubova, A. I. Gribenyukov, Y. P. Mironov. Two-temperature synthesis of ZnGeP₂. *Inorg. Mater.*, 2007, 43(10): 1040–1045

76. K. T. Zawilski, P. G. Schunemann, S. D. Setzler, T. M. Pollak. Large aperture single crystal ZnGeP₂ for high-energy applications. *J. Cryst. Growth*, 2008, 310(7–9): 1891–1896

77. G. A. Verozubova, A. I. Gribenyukov. Growth of ZnGeP₂ crystals from melt. *Crystallogr. Rep.*, 2008, 53(1): 158–163

78. Z. Lei, C. Zhu, C. Xu, B. Yao, C. Yang. Growth of crack-free ZnGeP₂ large single crystals for high-power mid-infrared OPO applications. *J. Cryst. Growth*, 2014, 389: 23–29

79. S. Wang, et al. Crystal growth and piezoelectric, elastic and dielectric properties of novel LiInS₂ crystal. *J. Cryst. Growth*, 2013, 362: 308–311

80. Q. Yu, Z. Gao, S. Zhang, W. Zhang, S. Wang, X. Tao. Second order nonlin-

ear properties of monoclinic single crystal BaTeMo$_2$O$_9$. *J. Appl. Phys.*, 2012, 111(1): 013506

81. J. Cheng, et al. Synthesis and growth of ZnGeP$_2$ crystals: Prevention of non-stoichiometry. *J. Cryst. Growth*, 2013, 362: 125–129

82. Y. Li, Z. Wu, X. Zhang, L. Wang, J. Zhang, Y. Wu. Crystal growth and terahertz wave generation of organic NLO crystals: OH1. *J. Cryst. Growth*, 2014, 402: 53–59

83. Y. Li, J. Zhang, G. Zhang, L. Wu, P. Fu, Y. Wu. Growth and characterization of DSTMS crystals. *J. Cryst. Growth*, 2011, 327(1): 127–132

84. X. Lin, G. Zhang, N. Ye. Growth and characterization of BaGa$_4$S$_7$: A new crystal for mid-IR nonlinear optics. *Cryst. Growth Des.*, 2009, 9(2): 1186–1189

85. J. Yao, et al. BaGa$_4$Se$_7$: A new congruent-melting IR nonlinear optical material. *Inorg. Chem.*, 2010, 49(20): 9212–9216

86. C. Stolzenburg, W. Schüle, I. Zawischa, A. Killi, D. Sutter. 700 W intracavity-frequency doubled Yb:YAG thin-disk laser at 100 kHz repetition rate. In: W. A. Clarkson, N. Hodgson, R. K. Shori, eds. *Proceedings of SPIE 7578, Solid State Lasers XIX: Technology and Devices.* San Francisco, CA, USA, 2010: 75780A

87. G. D. Goodno, et al. Investigation of β-BaB$_2$O$_4$ as a Q switch for high power applications. *Appl. Phys. Lett.*, 1995, 66(13): 1575–1577

88. C. Stolzenburg, A. Giesen, F. Butze, P. Heist, G. Hollemann. Cavity-dumped intracavity-frequency-doubled Yb:YAG thin disk laser with 100 W average power. *Opt. Lett.*, 2007, 32(9): 1123–1125

89. M. Roth, N. Angert, M. Tseitlin. Growth-dependent properties of KTP crystals and PPKTP structures. *J. Mater. Sci-Mater. El.*, 2001, 12(8): 429–436

90. M. Roth, M. Tseitlin, N. Angert. Oxide crystals for electro-optic Q-switching of lasers. *Glass Phys. Chem.*, 2005, 31(1): 86–95

91. Yu. V. Shaldin, S. Matyjasik, M. Tseitlin, M. Roth. Specific features of the pyroelectric properties of actual RbTiOPO$_4$ single crystals in the temperature range 4.2–300 K. *Phys. Solid State,* 2008, 50(7): 1315–1312

92. M. Roth, M. Tseitlin. Growth of large size high optical quality KTP-type crystals. *J. Cryst. Growth*, 2010, 312(8): 1059–1064

93. J. Y. Wang, et al. Progress of the electro-optic crystal research and the symmetry dependence of electro-optic effect. *Progress in Phys.*, 2012, 32(1): 33–56 (in Chinese)

94. L. Wang, X. Cai, J. Yang, X. Wu, H. Jiang, J. Wang. 520 mJ langasite electro-optically Q-switched Cr, Tm, Ho:YAG laser. *Opt. Lett.*, 2012, 37(11): 1986–1988

95. L. Wang, et al. 2.79 m high peak power LGS electro-optically Q-switched Cr, Er:YSGG laser. *Opt. Lett.*, 2013, 38(12): 2150–2152

96. M. Kiefer, F. Pröbst, G. Angloher, I. Bavykina, D. Hauff, W. Seidel. Glued CaWO$_4$ detectors for the CRESST-II experiment. *Opt. Mater.*, 2009, 31(10): 1410–1414

97. H. Kraus, et al. ZnWO$_4$ scintillators for cryogenic dark matter experiments. *Nucl. Instrum. Meth. A*, 2009, 600(3): 594–598

98. J. Chen, G. Zhao, D. Cao, S. Zhou. Color center of YAlO$_3$ with cation vacancies. *Curr. Appl. Phys.*, 2010, 10(2): 468–470

99. Q. Gui, C. Zhang, M. Zhang, L. Hang, Z. Fang, Y. Ge. Study on crystal growth and scintillation properties of large-size CeCl$_3$ doped LaBr$_3$ crystal. *Nuclear Electronics & Detection Technology*, 2011, 31(11): 1195–1197, 1249 (in Chinese)

100. Y. Zhang, M. Luo. Study on temperature characteristics of LaBr$_3$ detector. *Nuclear Electronics & Detection Technology*, 2013, 33(2): 188–190 (in Chinese)

101. Z. Ye. Relaxor ferroelectric Pb(Mg$_{1/3}$Nb$_{2/3}$)O$_3$: Properties and present understanding. *Ferroelectrics*, 1996, 184(1): 193–208

102. D. Viehland. Symmetry-adaptive ferroelectric mesostates in oriented Pb(BI$_{1/3}$BII$_{2/3}$)O$_3$-PbTiO$_3$ crystals. *J. Appl. Phys.*, 2000, 88(8): 4794–4806

103. G. A. Smolensky. Physical phenomena in ferroelectrics with diffused phase transition. *J. Phys. Soc. Jpn*, 1970, 28(Suppl.): 26–37

104. S. E. Park, T. R. Shrout. Ultrahigh strain and piezoelectric behavior in relaxor based ferroelectric single crystals. *J. Appl. Phys.*, 1997, 82(4): 1804–1811

105. K. Saitoh, Y. Ishimaru, H. Fuke, Y. Enomoto. A model analysis for current-voltage characteristics of superconducting weak links. *Jpn. J. Appl. Phys.*, 1997, 36(Part 2, No. 3A): L272–L275

106. L. Liu, et al. Dielectric, ferroelectric, and pyroelectric characterization of Mn-doped 0.74Pb(Mg$_{1/3}$Nb$_{2/3}$)O$_3$–0.26PbTiO$_3$ crystals for infrared detection applications. *Appl. Phys. Lett.*, 2009, 95(19): 192903

107. A. Borisevich, et al. Lead tungstate scintillation crystal with increased light yield for the PANDA electromagnetic calorimeter. *Nucl. Instrum. Meth. A*, 2005, 537(1–2): 101–104

108. S. Saitoh, M. Izumi, Y. Yamashita, S. Shimanuki, M. Kawachi, T. Kobayashi. Piezoelectric single crystal, ultrasonic probe, and array-type ultrasonic probe: US, 5402791A, 1995-04-04

109. B. Ren, S. W. Or, X. Zhao, H. Luo. Energy harvesting using a modified rectangular cymbal transducer based on 0.71Pb(Mg$_{1/3}$Nb$_{2/3}$)O$_3$–0.29PbTiO$_3$ single crystal. *J. Appl. Phys.*, 2010, 107(3): 034501

110. N. Neumann, M. Es-Souni, H. Luo. Application of PMN-PT in pyroelectric detectors. In: *Proceedings of the 18th IEEE International Symposium on the Applications of Ferroelectrics.* Xi'an, China, 2009: 1–3

111. Y. Wang, S. W. Or, H. L. W. Chan, X. Zhao, H. Luo. Magnetoelectric effect from mechanically mediated torsional magnetic force effect in NdFeB magnets and shear piezoelectric effect in 0.7Pb(Mg$_{1/3}$Nb$_{2/3}$)O$_3$–0.3PbTiO$_3$ single crystal. *Appl. Phys. Lett.*, 2008, 92(12): 123510

112. H. Luo, G. Xu, H. Xu, P. Wang, Z. Yin. Compositional homogeneity and electrical properties of lead magnesium niobate titanate single crystals grown by a modified bridgman technique. *Jpn. J. Appl. Phys.*, 2000, 39(Part 1, No. 9B): 5581–5585

113. P. Yu, et al. Growth and pyroelectric properties of high Curie temperature relaxor-based ferroelectric Pb(In$_{1/2}$Nb$_{1/2}$)O$_3$–Pb(Mg$_{1/3}$Nb$_{2/3}$)O$_3$–PbTiO$_3$ ternary single crystal. *Appl. Phys. Lett.*, 2008, 92(25): 252907

114. B. Gao, G. L. Yu, J. B. Li. Numerical simulation and experimental study on two-dimensional solid/fluid phononic crystals. *J. Synth. Cryst.*, 2010, 39(3): 680–686

115. Y. Gao, et al. Evolution and structure of low-angle grain boundaries in 6H-SiC single crystals grown by sublimation method. *J. Cryst. Growth*, 2010, 312(20): 2909–2913